© 2017. Published by The Company of Biologists Ltd | Journal of Cell Science (2017) 130, 2277-2291 doi:10.1242/jcs.192781

RESEARCH ARTICLE

Low-intensity pulsed ultrasound promotes cell motility through vinculin-controlled Rac1 GTPase activity

Paul Atherton[1], Franziska Lausecker[1], Andrew Harrison[2] and Christoph Ballestrem[1,*]

ABSTRACT

Low-intensity pulsed ultrasound (LIPUS) is a therapy used clinically to promote healing. Using live-cell imaging we show that LIPUS stimulation, acting through integrin-mediated cell-matrix adhesions, rapidly induces Rac1 activation associated with dramatic actin cytoskeleton rearrangements. Our study demonstrates that the mechanosensitive focal adhesion (FA) protein vinculin, and both focal adhesion kinase (FAK, also known as PTK2) and Rab5 (both the Rab5a and Rab5b isoforms) have key roles in regulating these effects. Inhibiting the link of vinculin to the actin-cytoskeleton abolished LIPUS sensing. We show that this vinculin-mediated link was not only critical for Rac1 induction and actin rearrangements, but was also important for the induction of a Rab5-dependent increase in the number of early endosomes. Expression of dominant-negative Rab5, or inhibition of endocytosis with dynasore, also blocked LIPUS-induced Rac1 signalling events. Taken together, our data show that LIPUS is sensed by cell matrix adhesions through vinculin, which in turn modulates a Rab5-Rac1 pathway to control ultrasound-mediated endocytosis and cell motility. Finally, we demonstrate that a similar FAK-Rab5-Rac1 pathway acts to control cell spreading upon fibronectin.

KEY WORDS: Vinculin, LIPUS, Rac1, Migration, Endocytosis

INTRODUCTION

Low-intensity pulsed ultrasound (LIPUS) is an externally applied therapeutic intervention used clinically to promote fracture healing (Gebauer et al., 2005; Heckman et al., 1994; Kristiansen et al., 1997; Nolte et al., 2001). LIPUS therapy consists of 20 min of daily stimulation targeted at the site of injury, with an unfocussed ultrasound transducer delivering 200 ms bursts of 1.5 MHz ultrasound pulsed at 1 kHz (Fig. S1A), to an intensity of 30 mW/cm^2 spatial average-temporal average (SATA), with a power of 117 mW (Harrison et al., 2016). LIPUS shows particular efficacy in treating bone nonunion fractures (Nolte et al., 2001; Rutten et al., 2007; Zura et al., 2015a), and has been approved by the US FDA for treating both fresh fractures and nonunion fractures, and by NICE in the UK for treating nonunion fractures (Higgins et al., 2014).

Many *in vivo* studies have demonstrated that LIPUS can be beneficial in improving healing in several other tissue types, including the skin wounds of diabetic and aged mice by increasing fibroblast migration into the wound site (Roper et al., 2015), ischemic heart disease by increasing angiogenesis (Hanawa et al., 2014), tendon repair (Jeremias Junior et al., 2011; Lu et al., 2016) by increasing collagen synthesis (Fu et al., 2010), and muscle repair after injury by increasing myofibre regeneration (Chan et al., 2010).

Despite this, little is known about the underlying molecular mechanisms. The ultrasound intensities used in LIPUS therapy are sufficiently low to prevent thermal effects (Mizrahi et al., 2012), suggesting that any cellular changes are caused by nonthermal effects. Previous studies, the majority of which have looked at the medium- to long-term (4–48 h) effects of LIPUS stimulation, have implicated integrin signalling pathways (Cheng et al., 2014; Sato et al., 2014; Xia et al., 2015; Zhou et al., 2004), ERK/MAPK signalling (Kusuyama et al., 2014) and GTPase activation (Mahoney et al., 2009). However, the precise mechanism by which cells sense LIPUS and the early signalling events (i.e. within minutes of stimulation) have yet to be clarified.

LIPUS stimulation can be considered to generate a type of external force acting upon cells (Padilla et al., 2014). The pulse modulation of the LIPUS signal produces motion occurring at a frequency of 1 kHz, and has been shown to produce tissue movement in the nanometre range (Harrison et al., 2016); replication of this motion has been shown to generate the same phenotype in chondrocytes as stimulation with LIPUS (Argadine et al., 2005). More recently, Veronick et al. (2016) showed that LIPUS stimulation induces movement of fluorescent beads encapsulated within a collagen hydrogel.

We aimed to investigate how the physical stimulation of cells with LIPUS is converted into biochemical signalling. The conversion of extracellular forces to intracellular signalling events is termed mechanotransduction; focal adhesions (FAs), which link the intracellular actin cytoskeleton to the ECM via integrins, are implicated as mechanosensitive cellular organelles (Puklin-Faucher and Sheetz, 2009; Schwarz and Gardel, 2012), capable of sensing forces and generating signalling events in response (Goldmann, 2012). The FA protein vinculin has been shown to be particularly important for mechanotransduction (Atherton et al., 2016); the link between vinculin and actin is required for cell polarization and Rac1 activation in response to cyclic stretching (Carisey et al., 2013), and vinculin is involved in generating cellular responses to different ECM rigidities (Holle et al., 2013; Rubashkin et al., 2014; Yamashita et al., 2014).

The GTPase Rac1 is an important regulator of the actin cytoskeleton, driving its polymerization and reorganization to facilitate cell migration (Ridley, 2011). Efficient wound healing requires cells to migrate into the injured site, requiring changes to cell motility; primary fibroblasts from patients with chronic wounds show reduced cell motility compared to healthy fibroblasts (Brem et al., 2008).

Here, we use live-cell imaging to show that LIPUS stimulation leads to dramatic rearrangement of the actin cytoskeleton and increased endocytosis, coupled with activation of Rac1 and Cdc42,

[1]Wellcome Trust Centre for Cell-Matrix Research, University of Manchester, Manchester M13 9PT, USA. [2]Bioventus Cooperatief, Taurusavenue 31, 2132 LS Hoofddorp, The Netherlands.

*Author for correspondence (christoph.ballestrem@manchester.ac.uk)

P.A., 0000-0003-3098-674X; C.B., 0000-0002-5375-7985

Received 23 May 2016; Accepted 29 May 2017

Journal of Cell Science

Journal of Cell Science (2017) 130, 2277-2291 doi:10.1242/jcs.192781

driving increased cell motility. Furthermore, we demonstrate that cell-ECM adhesions are critical for these responses, and that mechanosensing of LIPUS is mediated via the FA protein vinculin. We identify a novel role for vinculin in regulating Rab5 (both the Rab5a and Rab5b isoforms) and the recruitment of Rac1 to Rab5-positive vesicles, driving Rac1 activation to promote cell migration.

RESULTS

LIPUS induces circular ruffling and cell edge protrusions, and enhances cell motility

LIPUS promotes healing, which we hypothesized is likely caused by changes in actin dynamics, resulting in increased cell migration. To examine whether LIPUS affects actin dynamics, we used B16 melanoma cells stably expressing GFP-actin. These cells are ideal for actin-related studies as they are highly sensitive to changes in intracellular signalling, and undergo fast actin rearrangements (Ballestrem et al., 2000, 1998). LIPUS stimulation of these cells promoted the formation of actin-based circular dorsal ruffles (CDRs) which are associated with macropinocytosis (Dharmawardhane et al., 2000; Dowrick et al., 1993) and cell motility (Krueger et al., 2003; Sero et al., 2011; Suetsugu et al., 2003). CDR formation increased almost immediately upon stimulation, with the greatest number seen 10 min after the end of LIPUS stimulation (Fig. 1A; Movie 1). To determine if the actin-cytoskeletal response was limited to this cell type, we tested LIPUS on mouse embryonic fibroblasts (MEFs) expressing RFP-LifeAct for live-cell imaging. In these cells, which rarely form CDRs, LIPUS significantly increased the formation of cell membrane protrusions (Fig. 1B; Movie 2), resulting in cell shape reorganizations to a more polarized form with directional cell edge protrusions (Fig. 1C). These changes persisted until the end of imaging (20 min after the end of stimulation). Ultrasound stimulation increased the velocity of B16 cells and MEFs by 80% and 50%,

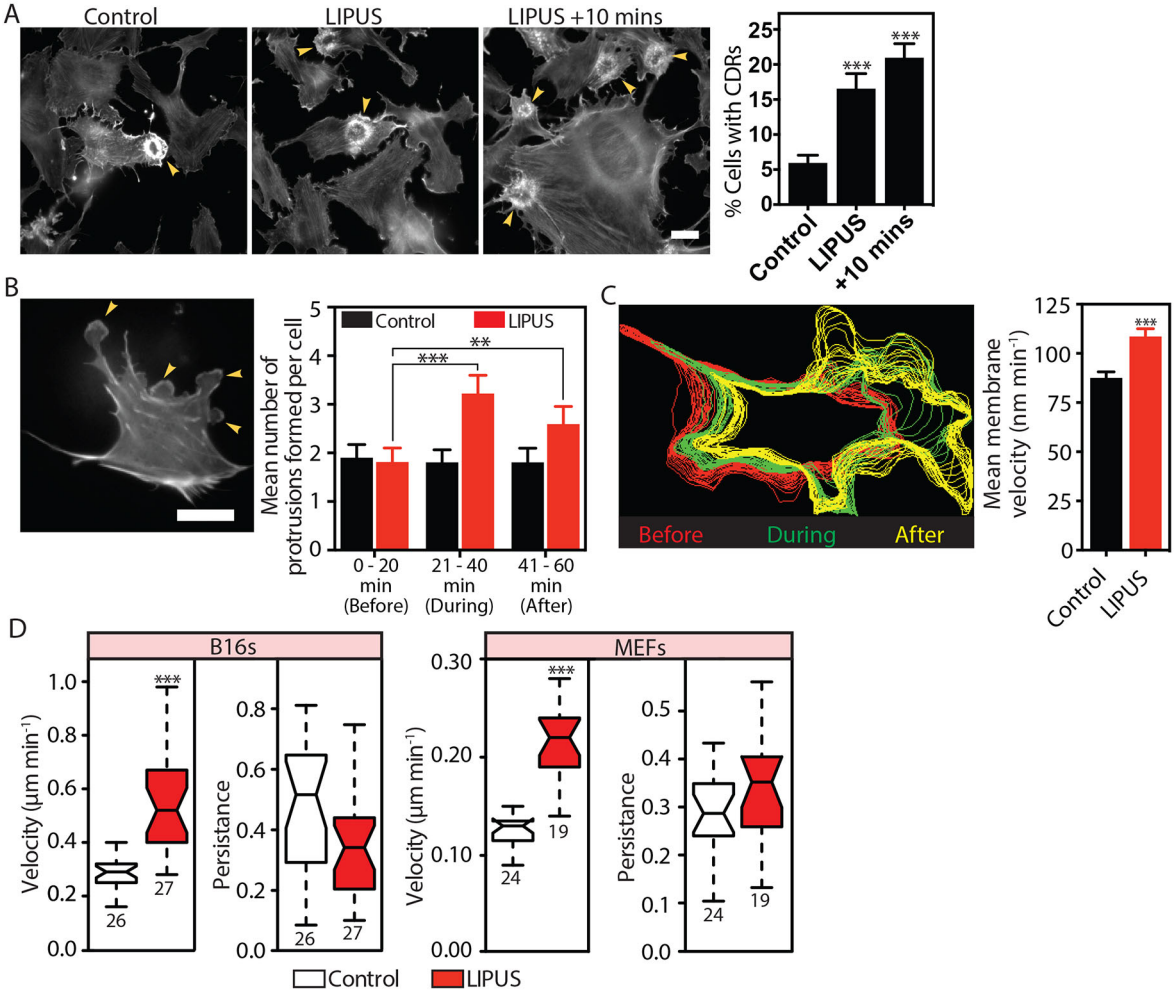

Fig. 1. LIPUS stimulation leads to rapid cytoskeleton rearrangement and increased cell motility. (A) B16 GFP-actin cells were fixed after receiving no LIPUS stimulation (control), immediately after the end of the 20 min stimulation (LIPUS) or 10 min after the end of the stimulation (LIPUS+10 min). Scale bar: 20 µm. Quantification of 60 randomly selected XY positions. Data are mean±s.e.m. from three independent experiments. Note the marked increase in CDRs after LIPUS (see also Movie 1). (B) MEFs expressing LifeAct were imaged for 1 h (Movie 2); LIPUS was started after 20 min. Scale bar: 50 µm. LIPUS stimulation increased the formation of small membrane protrusions, quantified by manual counting. Data are mean±s.e.m. from three independent movies; *n*=31 (control) and *n*=27 (LIPUS). (C) Automated detection of the cell periphery and quantification of membrane velocity using QuimP (Bosgraaf et al., 2009). The colour-coded shape outlines indicate representative protrusive activities recorded before (red), during (green), and after (yellow) LIPUS application. Note that the spacing between lines increases due to increases in protrusion velocity of LIPUS-stimulated MEFs compared to nonstimulated controls. Data are mean±s.e.m from three independent movies; *n*=69 (control) and *n*=63 (LIPUS). (D) Tracking of LIPUS-stimulated or nonstimulated control cells shows that LIPUS stimulation increases the velocity, but not persistence, of B16 and MEF cells (results are representative of three independent experiments and are presented as described in the Materials and Methods; *n* numbers are indicated below the plots). ***P*<0.01, ****P*<0.001.

Journal of Cell Science (2017) 130, 2277-2291 doi:10.1242/jcs.192781

respectively (Fig. 1D). However, the persistence of migration (Euclidean distance divided by accumulated distance) remained unchanged. The change in velocity occurred regardless of fibronectin concentration (Fig. S1B). Overall, we conclude that LIPUS induces actin rearrangements that lead to increased cell migration.

LIPUS induces the rapid activation of the Rho GTPases Rac1 and Cdc42

The Rho-family GTPases Rac1 and Cdc42 regulate actin protrusions and cell motility (Ridley, 2011), and are involved in CDR formation (Dharmawardhane et al., 2000). We used fluorescence resonance energy transfer (FRET)-based activation probes (Itoh et al., 2002) and live-cell imaging to measure the activation kinetics of these two GTPases following LIPUS stimulation. Temporal changes in FRET were monitored before, during and after LIPUS stimulation. LIPUS stimulation of B16 cells resulted in an almost immediate increase in Rac1 activation (Fig. 2A) with a slightly delayed activation of Cdc42 (Fig. 2B).

To determine whether Rac1 or Cdc42 activation is required for the LIPUS-induced formation of CDRs, we measured CDR formation in cells pretreated with either the Rac1 inhibitor EHT1864 (Onesto et al., 2008) or the Cdc42 inhibitor ML-141 (Surviladze et al., 2010). Although the Cdc42 inhibitor had no effect on the LIPUS-induced fourfold increase in CDR formation seen in control cells, this change was blocked by the Rac1 inhibitor EHT1864 (Fig. 2C). Similarly, LIPUS-induced migration of both B16 cells and MEFs was blocked by Rac1 inhibition (Fig. 2D). As LIPUS is primarily used clinically to promote the healing of bone injuries, we also tested the ability of LIPUS to stimulate the migration of MC3T3 cells, sourced from mice calvaria (Sudo et al., 1983). In these cells, similar to B16s and MEFs, LIPUS enhanced migration by ∼60%, an increase that was readily blocked by pretreatment with EHT1864 (Fig. S1D). Taken together, these data show that LIPUS rapidly induces Rac1 and Cdc42 activation, and it is Rac1 that mediates the observed LIPUS-induced actin cytoskeleton rearrangements and increased cell motility.

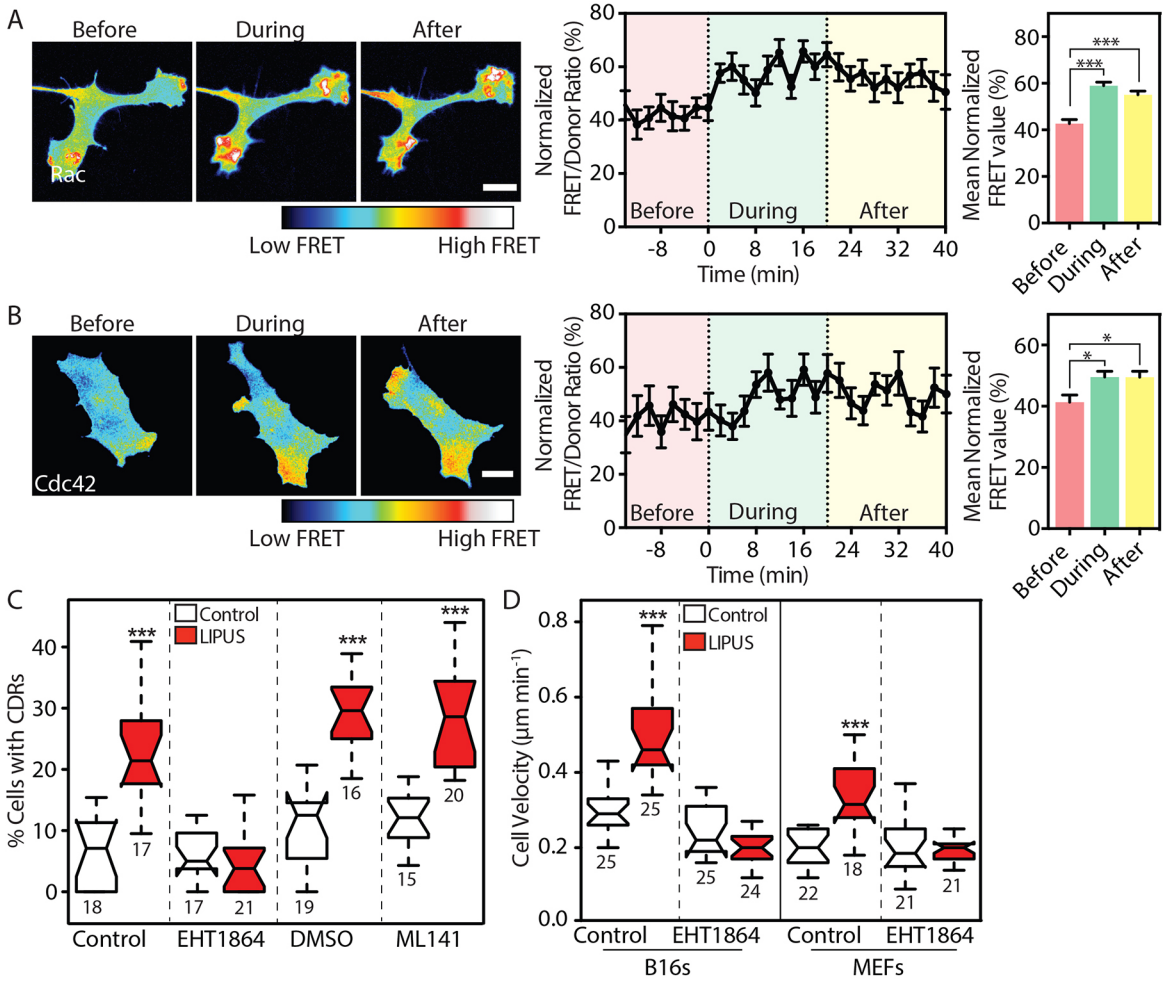

Fig. 2. LIPUS stimulates rapid GTPase activation and endocytosis. (A,B) B16 cells expressing (A) Rac1 or (B) Cdc42 FRET-based activity reporters were imaged before, during and after LIPUS stimulation. Images and quantifications of ratiometric FRET (normalized between 0 and 100 over time) analysis show that LIPUS stimulation leads to rapid activation of both GTPases, and that elevated GTPase activation persists after the stimulation ends. Scale bars: 10 µm. Data are mean±s.e.m. from three independent experiments; n=26 in A and n=17 in B. (C) Pretreatment of B16 cells with the Rac1 inhibitor EHT1864 (10 µM), but not with the Cdc42 inhibitor ML141 (10 µM), blocked LIPUS-induced CDR formation. Measurements are from the indicated numbers of XY positions, representative of three independent experiments. (D) Pretreatment with EHT1864 (10 µM) also blocked LIPUS-induced motility increases in both B16 and MEF cells. Cells were tracked over 16 h to assess cell motility (results are representative of three independent experiments and are presented as described in the Materials and Methods). *P<0.05, ***P<0.001.

Journal of Cell Science

Journal of Cell Science (2017) 130, 2277-2291 doi:10.1242/jcs.192781

LIPUS increases the number of early endosomes in a Rac1-dependent manner

While induction of CDRs and increased protrusive activity were the most striking effects of LIPUS, we also observed the formation of actin-positive 'comet-tail' structures during live imaging in B16 GFP-actin cells. These structures were particularly evident in cells that had previously been serum starved (Fig. 3A; Movie 3). Comet tails have previously been linked with the movement of endocytic vesicles (Merrifield et al., 1999), which led us to investigate whether LIPUS stimulation alters the number of endosomes within cells. LIPUS increased the number of early endosome antigen 1 (EEA1)-positive structures by ∼35% in nontransfected or wild-type Rac1-expressing B16 cells (Fig. 3B,C; Fig. S2A), supporting previous observations (Hauser et al., 2009). However, this increase in the number of early endosomes was inhibited by the expression of either dominant-negative (DN) ($Rac1^{N17}$) (Fig. 3C) or constitutively active (CA) ($Rac1^{L61}$) (Fig. 3D) Rac1, suggesting that a stimulus leading to changes in Rac1 activity levels is required to trigger endosome formation.

LIPUS-induced CDRs and early endosomes are dependent on cell interaction with the ECM

How cells sense LIPUS is unclear. As LIPUS has the potential to act as a physical force on cells (Argadine et al., 2005; Padilla et al., 2014), and FAs are known to be involved in mechanosensing (Geiger et al., 2009; Shemesh et al., 2005), we tested the possibility that FAs are involved in LIPUS sensing. B16 GFP-actin cells were seeded for 1 h on either fibronectin (an integrin ligand) or Cell-Tak (a substrate to which cells attach and spread in an integrin-independent manner) (Hwang et al., 2007). B16 GFP-actin cells on fibronectin, but not Cell-Tak, developed large FAs associated with actin stress fibres (Fig. 4A). Quantification of CDR formation showed that these dynamic actin structures were strongly induced by LIPUS in cells plated on fibronectin, but not in the cells on Cell-Tak (Fig. 4B). Although some cells on Cell-Tak did form CDRs, this only occurred in a fraction of cells that had begun to form adhesions (Fig. 4C), through *de novo* deposition of ECM proteins (Fig. S2B). Nevertheless, the adhesions present in these cells were not sufficient to induce a response to LIPUS, given that we observed no difference in the number of CDRs formed within this population. These data demonstrate that integrin-mediated adhesions are critical for LIPUS-induced formation of CDRs. As for CDR formation, we found that an increase in the number of EEA1-positive endosomes after LIPUS stimulation only occurred in cells on fibronectin and not in those on Cell-Tak (Fig. 4D,E) Interestingly, after 1 h of spreading, the cells on Cell-Tak had ∼50% fewer EEA1-positive vesicles than those on fibronectin. Taken together, these data show that integrin-mediated adhesions are essential for sensing LIPUS. Furthermore, our results suggest a link between cell-ECM adhesions and both CDR formation and endocytosis.

Sensing of LIPUS is mediated through vinculin and its link to actin

The above experiments show that integrin-associated signals are involved in the sensing of LIPUS. The adapter protein vinculin is an important protein involved in the transduction of mechanical signals (Carisey et al., 2013; Humphries et al., 2007; Thompson et al., 2014). To test the role of vinculin in LIPUS sensing, we first examined whether LIPUS can activate Rac1 in vinculin knockout MEFs ($vin^{-/-}$ MEFs). Interestingly, cells lacking vinculin showed no increase in Rac1 activity during or after LIPUS stimulation

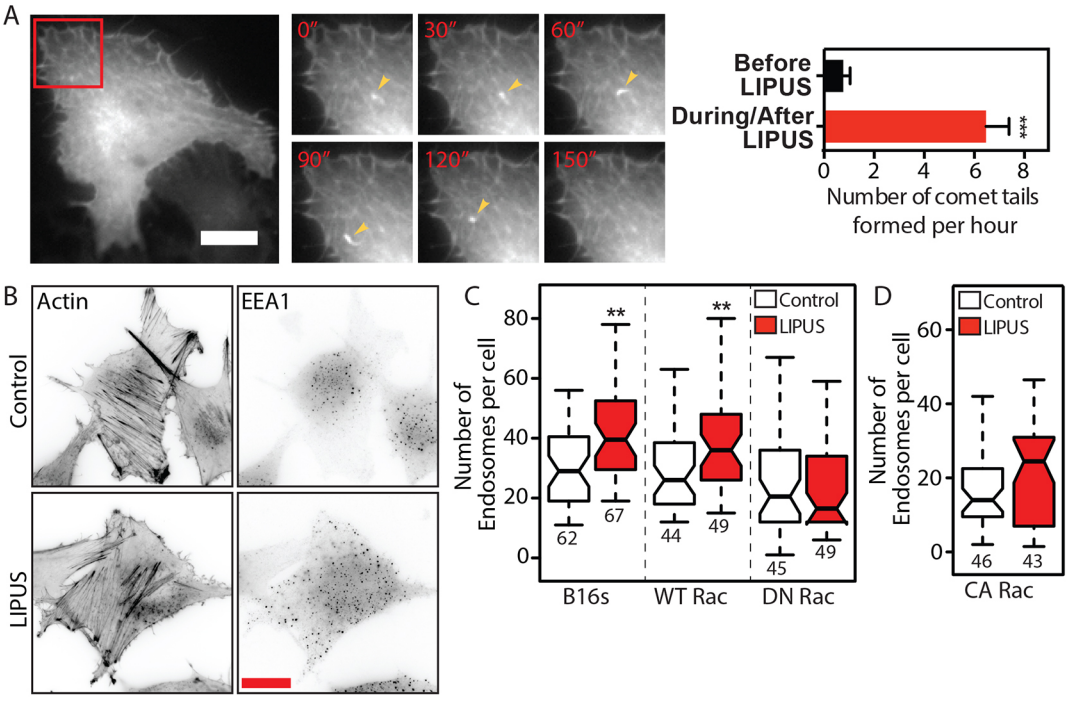

Fig. 3. LIPUS increases the number of early endosomes in a Rac1-dependent manner. (A) LIPUS stimulation in serum-starved B16 GFP-actin cells leads to the formation of actin comet-tails (arrowheads). The inset is shown in higher magnification in the right-hand panels at the indicated times (min). Data are mean±s.e.m. from three independent movies; n=17. Scale bar: 20 µm. (B) Immunofluorescence images (colour inverted) of B16 cells with or without LIPUS stimulation, stained for actin or EEA1. Scale bar: 20 µm. (C) Quantification of the number of endosomes in B16 control cells or cells expressing WT Rac1 or DN Rac1. Note that the expression of DN Rac1 blocks the LIPUS-induced increase in early endosomes. (D) Expression of CA Rac1 also prevents any change in the number of EEA1-positive early endosomes after LIPUS stimulation. Data in C and D are from three independent experiments and are presented as described in the Materials and Methods. $^{**}P$<0.01.

Journal of Cell Science (2017) 130, 2277-2291 doi:10.1242/jcs.192781

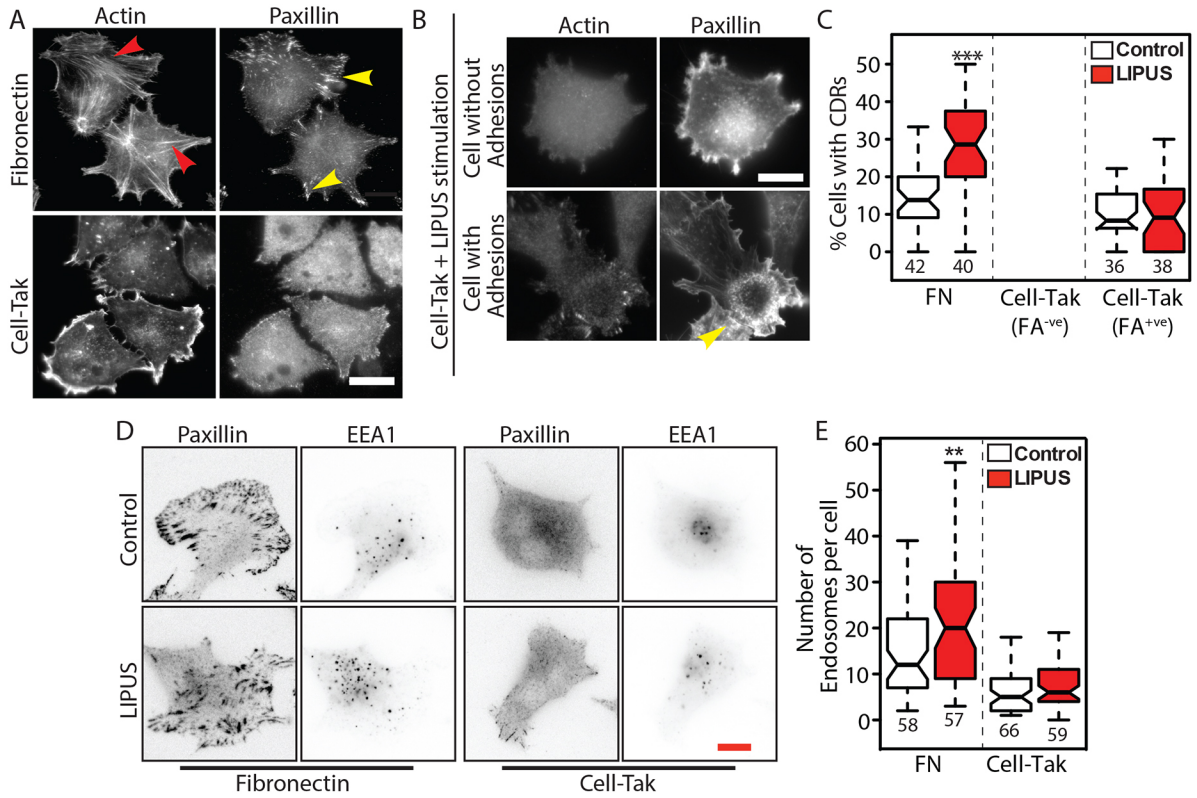

Fig. 4. Cell-ECM adhesions are required for LIPUS-induced CDR formation and increases in early endosomes. (A,B) Cells were seeded on fibronectin or Cell-Tak coated glass and stained for actin and the FA marker paxillin. Cells on fibronectin form FAs (yellow arrowheads), connected to actin stress fibres (red arrowheads), whereas the majority of cells on Cell-Tak did not form any adhesions. In some cases, cells on Cell-Tak were able to form adhesions. Scale bar: 20 µm. (C) LIPUS stimulation of cells on fibronectin (FN) produced an increase in the number of cells with CDRs, but LIPUS stimulation had no effect on CDR formation in cells on Cell-Tak, including those that had formed some small adhesions. (D) Control and LIPUS-treated cells on either fibronectin or Cell-Tak and stained for paxillin and EEA1 (colour inverted). Scale bar: 10 µm. (E) Quantification of the number of early endosomes in LIPUS-stimulated and control cells on FN- or Cell-Tak-coated glass. Note that LIPUS-stimulation had no effect on the number of early endosomes in the cells on Cell-Tak. Data in C and E are from three independent experiments and are presented as described in the Materials and Methods; *n* numbers are indicated below the plots. $^{**}P<0.01$, $^{***}P<0.001$.

(Fig. 5A). This response was rescued by expressing a wild-type vinculin (vinFL) construct (Fig. 5A). These data show that LIPUS-induced Rac1 activation requires vinculin.

Next, we assessed the motility of vin$^{-/-}$ MEFs or vin$^{-/-}$ MEFs expressing GFP-vinculin with or without LIPUS stimulation. LIPUS stimulation caused a 30% increase in migration speed (0.2 to >0.3 µm/min) in cells expressing GFP-vinculin compared to untreated cells, which was readily blocked by the Rac1 inhibitor EHT1864 (Fig. 5B). As reported previously, vin$^{-/-}$ cells migrated faster than those expressing vinculin (Saunders et al., 2006), but LIPUS caused no further increase in migration speed in these cells (Fig. 5B). This was observed even at very low fibronectin concentrations (Fig. S3A). Interestingly, the absence of vinculin not only blocked LIPUS-induced Rac1 activation and increased cell velocity, but also blocked the LIPUS-induced increase in early endosomes, which was rescued in cells expressing vinFL (Fig. 5C). This increase was also Rac1 dependent, as it was readily blocked by EHT1864 (Fig. S2C,D).

To investigate whether LIPUS stimulation directly affects the dynamics of vinculin within the FA, we used fluorescence loss after photoactivation (FLAP) (Atherton et al., 2015) to investigate the turnover of photoactivatable GFP (PAGFP)-vinculin before and during LIPUS stimulation. For these experiments, we used NIH3T3 fibroblasts. NIH3T3 fibroblasts are an ideal cell line for photokinetics experiments as they have large, prominent FAs, better transfection efficiency (than vin$^{-/-}$ MEFs) and ideal expression levels of PAGFP constructs. The results showed that vinculin turnover is strongly reduced in cells undergoing stimulation (Fig. 5D; Fig. S3C).

The link between vinculin and actin has been shown to be critical for the function of vinculin as a transducer of mechanical stimuli (Carisey et al., 2013; Thompson et al., 2014). To test whether this link is also critical for sensing LIPUS, we performed rescue experiments with vin$^{-/-}$ MEFs expressing vinFL^{I997A}, a point mutant with reduced actin binding (Thievessen et al., 2013). LIPUS could not increase Rac1 activity in these cells (Fig. 5E), nor could it increase their migration speed (Fig. 5F) or the number of EEA1-positive endosomes (Fig. S3D). Taken together, these results indicate that vinculin, and its actin-binding tail, is a critical mechanosensor of the LIPUS signal.

Focal adhesion kinase regulates the cellular response to LIPUS after the initial mechanosensing by vinculin

Focal adhesion kinase (FAK, also known as PTK2) is as an important component of cellular mechanotransduction, capable of generating intracellular signalling events in response to mechanical stimuli (Bae et al., 2014; Swaminathan et al., 2016). Therefore, we hypothesized that FAK signalling, downstream of the initial sensing of LIPUS by vinculin, is involved in Rac1 activation. First, we assessed levels of phosphorylated FAK (pFAK-Y397) in whole cell lysates of B16 cells stimulated with LIPUS for different periods of time, and found that pFAK-Y397 levels increased over time, peaking after 10 min of stimulation (Fig. 6A).

Journal of Cell Science (2017) 130, 2277-2291 doi:10.1242/jcs.192781

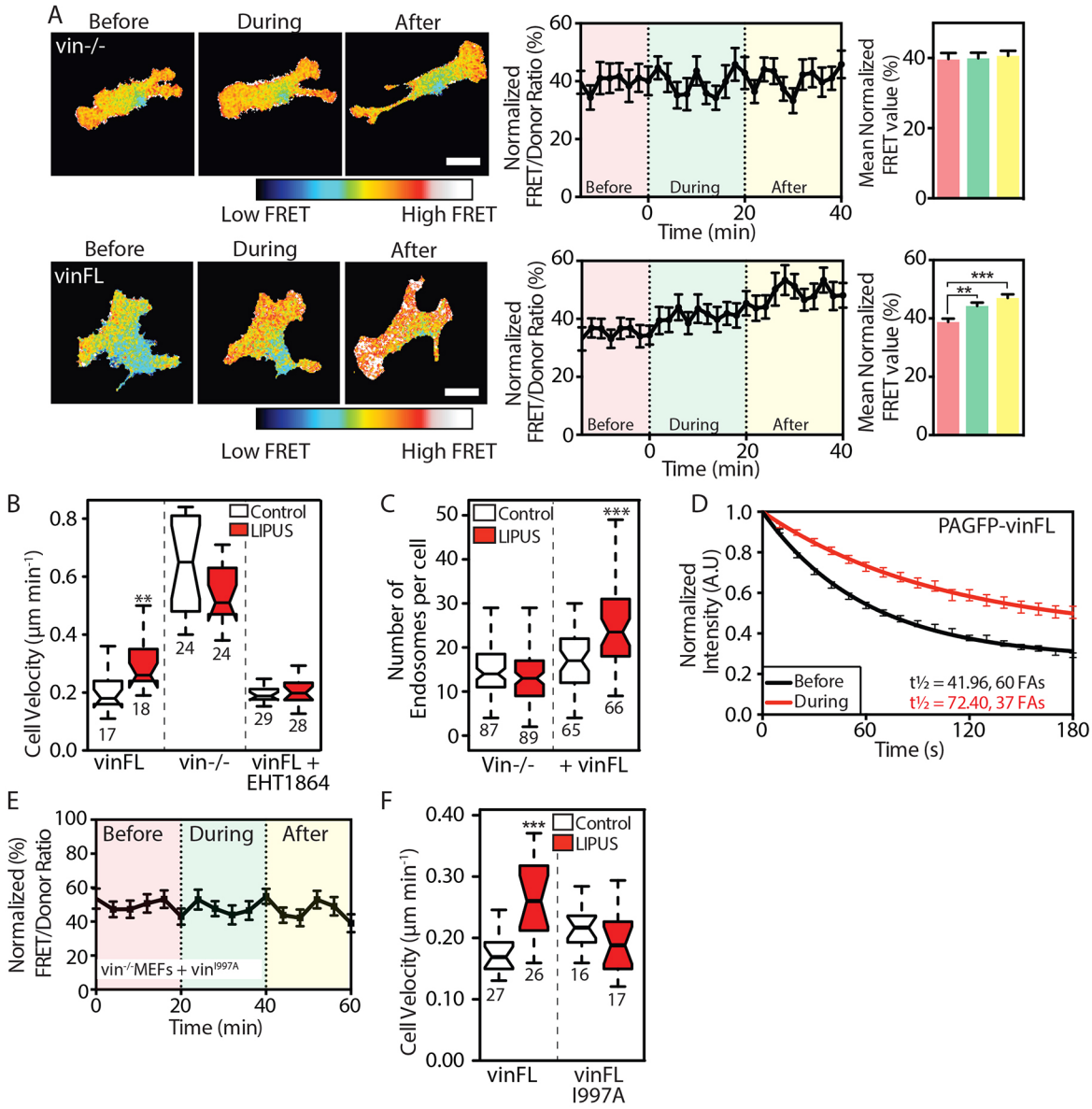

Fig. 5. Vinculin and its actin-binding potential are required for sensing LIPUS stimulation. (A) FRET measurements from vin$^{-/-}$ MEFs expressing the Raichu Rac1 FRET probe without (upper row) or with (lower row) vinFL. An increase in FRET signal in response to LIPUS is only seen in cells coexpressing mCherry-vinFL. Scale bars: 10 µm. Data are mean±s.e.m. from four independent experiments; *n*=26 (vin$^{-/-}$) and *n*=46 (vinFL). (B) LIPUS-stimulated vin$^{-/-}$ MEFs show no change in migration speed. Expression of vinFL rescues LIPUS-enhanced motility, which is blocked by pretreatment with the Rac1 inhibitor EHT1864 (10 µM). (C) The increase in the number of early endosomes after LIPUS stimulation is blocked in vin$^{-/-}$ MEFs, but rescued by expression of vinFL. (D) The turnover of PAGFP-vinculin was assessed using FLAP, before or during LIPUS stimulation. Data are mean±s.e.m. from at least three independent experiments. (E) FRET measurements from vin$^{-/-}$ MEFs coexpressing Raichu Rac1 and mCherry-vinFL^{I997A}. Note the lack of increase in FRET signal in response to LIPUS. Data are mean±s.e.m. from three independent experiments; *n*=32. (F) Vin$^{-/-}$ MEFs expressing vinFL^{I997A} show no change in motility after LIPUS stimulation. Results in B and F are representative of three independent experiments; results in C are from three independent experiments. Data are presented as described in the Materials and Methods; *n* numbers are indicated below the plots. ***P*<0.01, ****P*<0.001.

We hypothesized that FAK inhibition would block the cellular response to LIPUS. Cells were pretreated with a recently characterized FAK inhibitor (AZ13256675, referred to as FAKi), which dramatically reduced levels of pFAK-Y397 and blocked the LIPUS-induced increase in levels of pFAK-Y397 seen in DMSO-treated cells after 10 min of stimulation (Fig. 6B). We and others have recently shown that pretreatment with 3 µM FAKi for 1 h reduces tyrosine phosphorylation at FAs in NIH3T3 and HFF cells, without affecting the molecular composition of FAs or vinculin turnover (Horton et al., 2016; Stutchbury et al., 2017).

Pretreatment with 3 µM FAKi for 1 h blocked Rac1 activation in response to LIPUS stimulation (Fig. 6C), as well as the increase in the number of EEA1-positive early endosomes (Fig. 6D) and the increase in cell velocity after LIPUS stimulation (Fig. 6E). In accordance with previously published results, FAK inhibition reduced cell velocity (Horton et al., 2016). FAK inhibition also blocked the increased migration seen after LIPUS stimulation in MC3T3 cells, suggesting that this is a universal mechanism (Fig. S3E).

Finally, we aimed to determine whether FAK signalling occurs before or after the initial mechanosensing of LIPUS by vinculin. FLAP experiments repeated in cells pretreated with FAKi

Journal of Cell Science (2017) 130, 2277-2291 doi:10.1242/jcs.192781

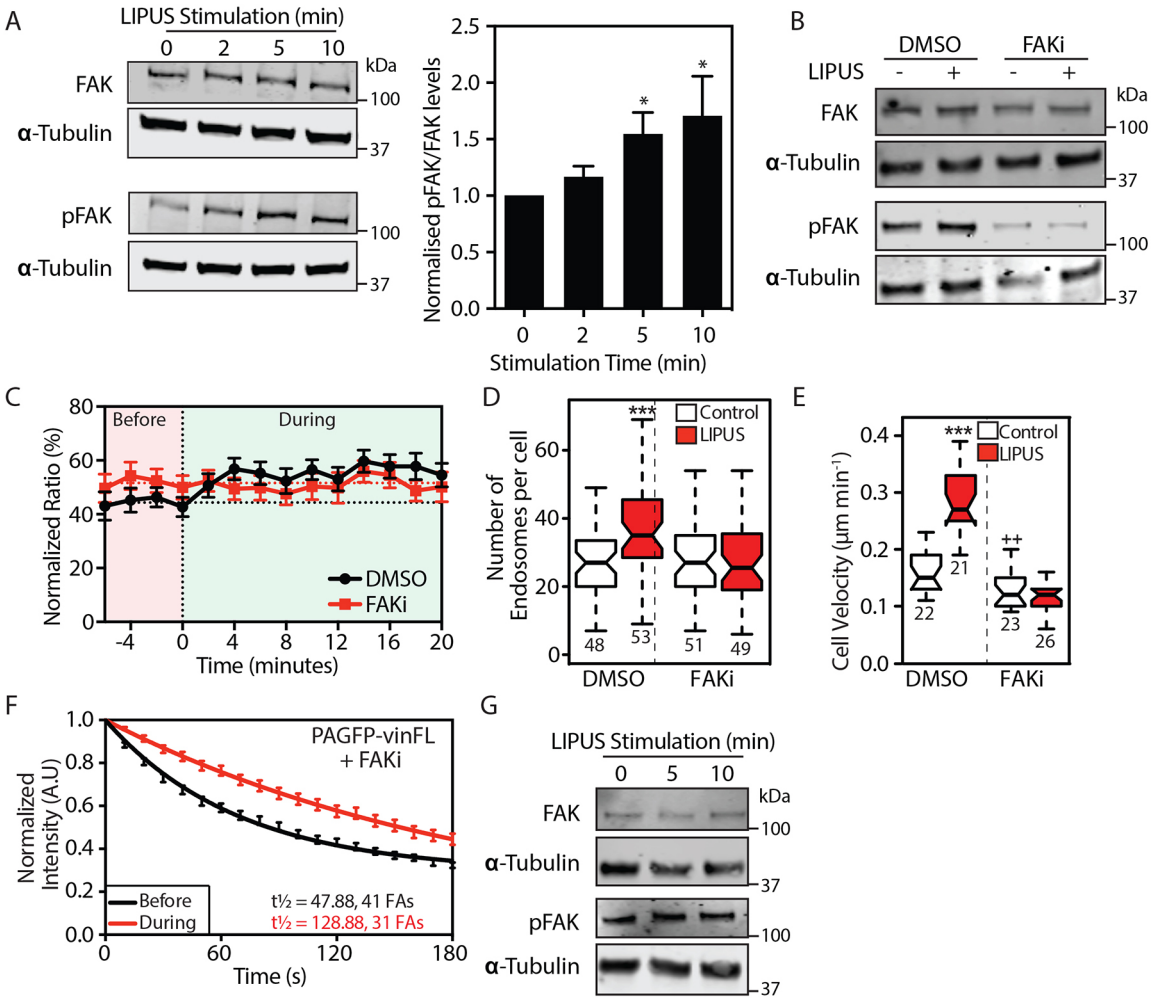

Fig. 6. FAK signalling regulates the cellular responses following mechanosensing of LIPUS by vinculin. (A) B16 cells were stimulated with LIPUS for 0, 2, 5 or 10 min and then lysed. The western blots show an increase in the amount of pFAK-Y397 relative to total FAK, with the maximum increase seen after 10 min of stimulation. The bar graph shows pFAK/FAK ratios from four independent experiments. **P*<0.05 (one-way ANOVA). (B) Pretreatment with 3 μM FAKi for 1 h dramatically reduces FAK phosphorylation levels, and also blocks the LIPUS-induced increase in pFAK-Y397 levels (cells were lysed after 10 min of stimulation). The western blots shown are representative of three independent experiments. (C) Raichu Rac1 FRET experiments were performed in cells pretreated with 3 μM FAKi or an equivalent volume of DMSO. FAK inhibition blocks the LIPUS-dependent increase in Rac1 activation. Data are mean±s.e.m. from three independent experiments; *n*=32 (DMSO) and *n*=26 (FAKi). (D) FAK inhibition also blocked the increase in the number of EEA1-positive endosomes after LIPUS stimulation (data are from three independent experiments), and (E) blocked the increase in cell velocity seen after LIPUS stimulation (data are representative of three independent experiments). Results are presented as described in the Materials and Methods, *n* numbers are indicated below the plots). (F) The turnover of PAGFP-vinFL was assessed using FLAP, before or during LIPUS stimulation, in the presence of 3 μM FAKi. In cells undergoing stimulation, the turnover of vinculin is reduced, even when FAK signalling is suppressed. Results are representative of at least three independent experiments. (G) Western blots of pFAK-Y397 and FAK in vin$^{-/-}$ MEFs stimulated with LIPUS for the indicated amount of time. Note that there is no increase in FAK phosphorylation in these cells (blots are representative of four independent experiments). α-Tubulin was used as a loading control. **P*<0.05, ****P*<0.001.

demonstrated that LIPUS stimulation reduced the turnover of vinculin even in the presence of FAKi (Fig. 6F; Fig. S3F). Furthermore, an increase in levels of pFAK-Y397 was not seen in vin$^{-/-}$ MEFs after LIPUS stimulation (Fig. 6G). Taken together, these results show that LIPUS promotes Rac1 activation in a FAK-dependent manner, thereby increasing cell motility. FLAP experiments show that the initial 'sensing' of LIPUS occurs independently of FAK and Rac1, resulting in altered turnover of vinculin.

Integrin internalization contributes to Rac1 signalling in response to LIPUS

Recycling of integrins from cell-ECM adhesions to the leading edge is one important facet of cell migration (Paul et al., 2015). To determine whether the EEA1-positive vesicles seen after LIPUS stimulation contained integrins, we expressed GFP-α5 integrin in vin$^{-/-}$ MEFs with or without CFP-vinculin coexpression. Immunostaining for EEA1 revealed that many of the EEA1-positive early endosomes colocalized with GFP-α5 integrin (Fig. 7A). This colocalization was only seen in cells seeded on an α5 ligand (i.e. fibronectin); it was not observed in cells on collagen (Fig. S3G). The number of GFP-α5 positive vesicles increased upon LIPUS stimulation (Fig. 7B). This increase was not seen in vin$^{-/-}$ MEFs, which interestingly had more GFP-α5-positive vesicles under control conditions than vinFL-expressing cells.

Since integrin trafficking has also been linked to Rac1 activation (Sandri et al., 2012), we examined whether the observed integrin internalization and endocytosis contributes to Rac1 signalling. Integrin internalization is dynamin dependent, and can be blocked by the dynamin inhibitor dynasore (Alanko et al., 2015). Pretreating

Journal of Cell Science (2017) 130, 2277-2291 doi:10.1242/jcs.192781

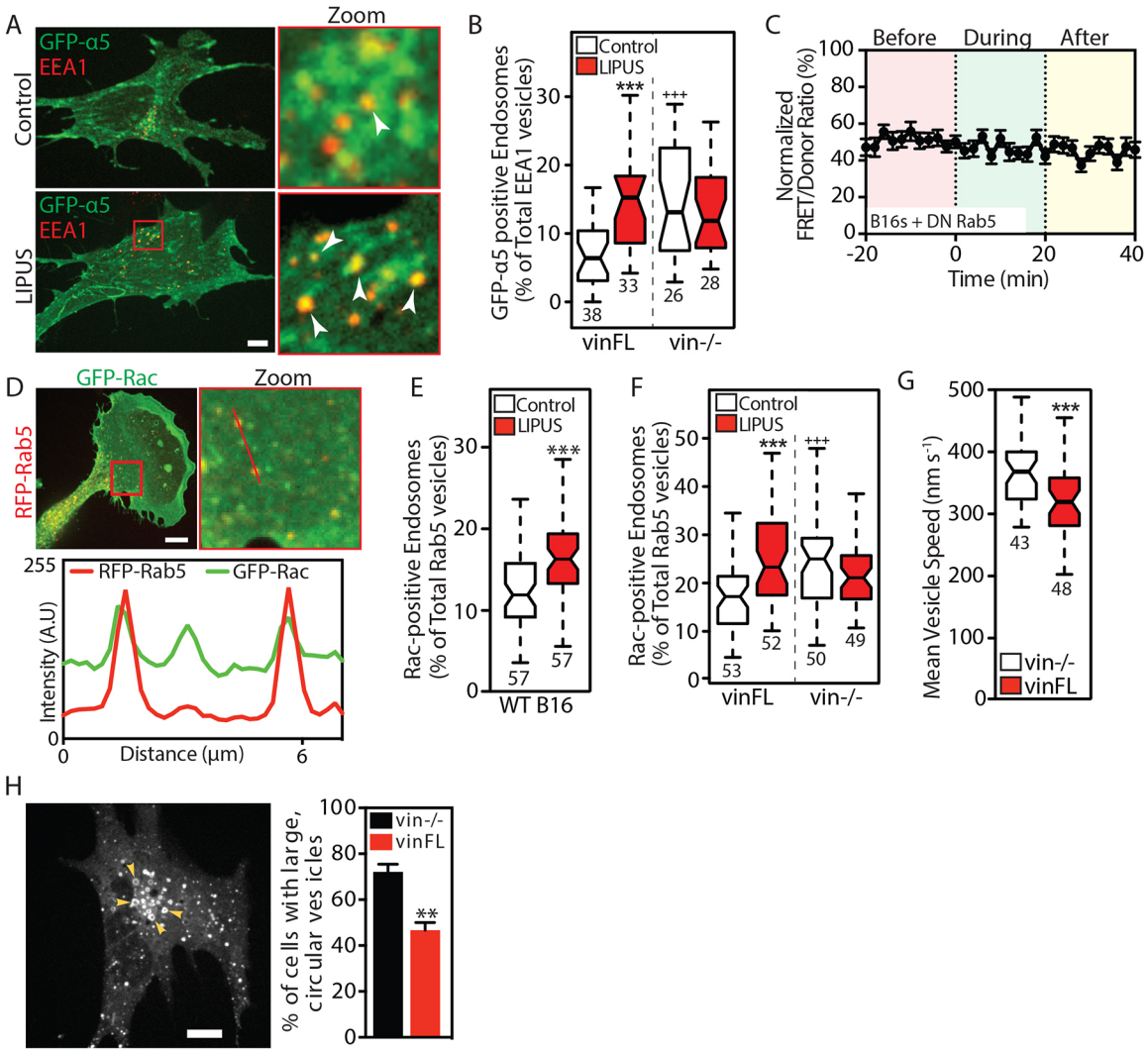

Fig. 7. Vinculin modulates Rab5-mediated Rac1 activation in response to LIPUS. (A) Confocal images of vin$^{-/-}$ MEFs rescued with CFP-vinculin and coexpressing GFP-α5 integrin, without (top row) or with (bottom row) LIPUS stimulation, fixed and stained for EEA1. Arrowheads indicate colocalization between GFP-α5 and EEA1. Scale bar: 10 µm. (B) Colocalization between GFP-α5 and EEA1 in cells fixed 10 min after the end of LIPUS stimulation. ***P<0.001 against the control; ^{+++}P<0.001 against the vinFL control. (C) LIPUS stimulation has no effect on Rac1 activity in B16 cells expressing DN Rab5 (Rab5^{S34N}) (data are mean±s.e.m.; n=37 from three independent experiments). (D) Confocal images of GFP-Rac1 and RFP-Rab5 expressed in B16 cells, with a line profile showing the colocalization of Rac1 and Rab5-positive vesicles. Scale bar: 10 µm. (E) Percentage of Rac1-positive Rab5 vesicles in control (white) and LIPUS-stimulated (red) B16 cells. (F) The recruitment of Rac1 to Rab5-positive vesicles in LIPUS-stimulated MEFs is only seen in vinculin-expressing cells (i.e. is vinculin dependent). Data are mean±s.e.m. from three independent experiments; n numbers are indicated below the plots. ***P<0.001 against the control; ^{+++}P<0.001 against the vinFL control. (G) Vesicle dynamics. Note that Rab5-positive vesicles move faster in vin$^{-/-}$ MEFs compared to vin$^{-/-}$ MEFs rescued with vinFL (see Movie 4). (H) Image of a vin$^{-/-}$ MEF expressing RFP-Rab5 (WT). Arrowheads indicate large, circular vesicles. Scale bar: 10 µm. The bar graph shows the (mean±s.e.m., three independent experiments) percentage of vin$^{-/-}$ and vinFL cells with large, circular vesicles. Results in B, E and F are from three independent experiments; results in G are representative of three independent experiments. Data are presented as described in the Materials and Methods; n numbers are indicated below the plots. **P<0.01, ***P<0.001.

cells with dynasore (80 µM) prevented LIPUS-induced EEA1 vesicle formation (Fig. S4A), as well as Rac1 activation (Fig. S4B) and the associated increase in cell motility (Fig. S4C). We therefore conclude that the LIPUS-induced internalization of the integrin-associated complex contributes to Rac1 activation and regulation of cell motility.

Rac1 activation requires functional Rab5

Upon internalization, integrins enter Rab5-positive endosomes (Ezratty et al., 2009; Pellinen et al., 2006; Roberts et al., 2001), before undergoing either recycling (back to the membrane) or degradation. Rab5 is a GTPase that regulates endocytosis, previously shown to associate vinculin (Hagiwara et al., 2014; Mendoza et al., 2013); Rab5-positive vesicles also act as platforms for Rac1 trafficking to promote CDR formation (Lanzetti et al., 2004; Palamidessi et al., 2008). Since our results demonstrate that LIPUS promotes the formation of both endosomes and CDRs, we hypothesized that Rac1 activation after LIPUS stimulation may require Rab5. LIPUS was unable to increase Rac1 activation in cells expressing DN Rab5 (Fig. 7C), confirming that Rac1 activation requires functional Rab5. Similarly, LIPUS was unable to increase the number of endosomes present in cells expressing DN Rab5 (Fig. S4D).

Similar to cells stimulated with growth factors (Palamidessi et al., 2008), we found that GFP-Rac1 and RFP-Rab5 colocalized in B16 cells (Fig. 7D) (Pearson's R 0.731±0.01 s.e.m, n=20), and that LIPUS stimulation increased the number of Rac1- and

Rab5-positive vesicles (Fig. 7E; Fig. S4E). A reporter for active Rac1 localization (YFP-CRIB-CFP) localized to Rab5-positive vesicles (Fig. S4F), demonstrating that Rac1 at endosomes is active, which is in agreement with the findings of Palamidessi et al. (2008).

Surprisingly, vin$^{-/-}$ cells showed an increase in the localization of Rac1 to Rab5-positive endosomes compared to vin$^{-/-}$ cells rescued with CFP-vinFL (Fig. 7F; Fig. S4G). Moreover, LIPUS stimulation had no effect on Rac1-Rab5 colocalization in vin$^{-/-}$ cells, compared with the increased colocalization seen in cells expressing vinFL (Fig. 7F), suggesting that this colocalization occurs after the initial sensing of LIPUS by vinculin. Consistent with this hypothesis, the increased colocalization seen between Rac1 and Rab5 in LIPUS-stimulated cells was blocked by pretreatment with FAKi (Fig. S4H).

Adhesion signalling has previously been linked to the endosomal compartment (Mendoza et al., 2013; Sandri et al., 2012); therefore we sought to determine whether the absence of vinculin affects Rab5 vesicles. Live-cell imaging revealed that Rab5-positive vesicles moved significantly faster (Fig. 7G; Movie 4) in vin$^{-/-}$ cells than in cells rescued with GFP-vinFL, suggesting that vinculin acts to suppress Rab5-positive vesicle motility. Furthermore, Rab5 endosomes had a markedly different morphology in vin$^{-/-}$ cells, with an increase in enlarged vesicles reminiscent of later endosomal compartments (Fig. 7H), suggestive of aberrant early endosomal maturation in the absence of FA signalling. Moreover, we confirmed previous observations that RFP-Rab5 localizes in proximity to FAs (Mendoza et al., 2013) (Fig. S4J).

Taken together, these results demonstrate that the behaviour of Rab5-positive vesicles is modulated by vinculin and that LIPUS-induced activation of Rac1 requires functional Rab5. Furthermore, LIPUS stimulation promotes the recruitment of Rac1 to Rab5-positive vesicles, and we wondered whether this is a phenotype that could be mimicked by integrin internalization. Interestingly, similarly to LIPUS, the addition of soluble fibronectin (10 µg/ml) increased Rac1-Rab5 colocalization (Fig. S4I). The amount of internalisation was dependent on the presence of vinculin; in vinculin$^{-/-}$ cells, Rac1-Rab5 colocalization was high independently of the presence of soluble fibronectin. These data suggest that vinculin contributes in a similar manner to the regulation of both LIPUS and fibronectin-induced receptor internalization and downstream Rac1 activation.

FAK, Rac1 and Rab5 are required for efficient cell spreading

Our results outline a pathway involving FAK, Rac1 and Rab5 acting downstream of cell-ECM adhesions in response to LIPUS to generate changes in the actin cytoskeleton and cell motility. We aimed to investigate whether a similar mechanism exists for an alternative FAK-dependent process: cell spreading on fibronectin (Owen et al., 1999). B16 cells were cotransfected with different combinations of wild-type (WT) or DN Rac1 and Rab5, and treated for 1 h in suspension with either DMSO or FAKi. Cell area was measured 45 min after plating onto fibronectin-coated (10 µg/ml) glass. FAKi-treated cells coexpressing both WT Rac1 and WT Rab5 were ∼40% smaller than DMSO-treated control cells, and were significantly rounder (Fig. 8A,B). Expression of either DN Rac1 or DN Rab5 also reduced cell area in DMSO-treated cells, indicating that both GTPases are required for cell spreading downstream of FAK activation after engagement of integrins with fibronectin (Fig. 8A).

To determine whether Rab5 acts upstream or downstream of Rac1, these experiments were repeated in cells coexpressing CA Rac1 with either WT or DN Rab5 (Fig. 8C). In cells coexpressing CA Rac1 and WT Rab5, FAK inhibition had no effect on cell area or circularity (Fig. 8D). Interestingly, cells coexpressing CA Rac1 and DN Rab5 were significantly smaller, suggesting that functional Rab5 supports cell spreading on fibronectin, which occurs in a Rac1-dependent manner. Finally, we also tested whether dynamin inhibition would mimic coexpression of DN Rab5. Cells coexpressing WT Rac1 and WT Rab5, or CA Rac1 and WT Rab5, were pretreated with dynasore in suspension before being plated onto fibronectin-coated plastic. As with expression of DN Rab5, dynasore treatment reduced cell spreading in both WT and CA Rac1-expressing cells (Fig. 8E).

Taken together, these results outline a mechanism whereby integrin-mediated FAK activation activates Rac1 in a Rab5-dependent manner, leading to actin rearrangements and cell spreading. To determine how these results fit with our observations of the effects of LIPUS on cells, we assessed whether LIPUS was able to induce an increase in the levels of pFAK-Y397 when either Rac1 or dynamin were inhibited. Interestingly, treatment with either EHT1864 or dynasore (Fig. 8F) prevented FAK phosphorylation after 10 min of LIPUS stimulation. Given that Rac1 activation in response to LIPUS stimulation was also blocked by dynasore treatment (Fig. S4B), we propose that a similar mechanism occurs downstream of the initial sensing of the LIPUS signal by vinculin (Fig. 8G). The finding that Rac1 inhibition prevented LIPUS-induced FAK phosphorylation suggests that there are feedback mechanisms driving this response to the stimulus.

DISCUSSION

The clinical benefits of LIPUS therapy are well documented (Gebauer et al., 2005; Heckman et al., 1994; Zura et al., 2015a,b), but the underlying molecular mechanisms remain poorly defined. Here, we show that LIPUS leads to an increased number of early endosomes, actin remodelling and, ultimately, enhanced cell migration. Mechanistically, these are all dependent on the activation of Rac1, which occurs rapidly upon the application of LIPUS. These LIPUS-induced effects are dependent on integrin-mediated adhesions and the associated FA protein vinculin and its interaction with actin.

Promotion of cell motility by LIPUS stimulation

Enhanced cell migration is a widely reported response to LIPUS stimulation, occurring in several cell types including mesenchymal stem cells (Wei et al., 2014), chondrogenic progenitor cells (Jang et al., 2014), primary human endothelial cells (Katano et al., 2011), human chondrocytes (Uddin et al., 2016) and MC3T3 mouse osteoblasts (Fig. S1C) (Sawai et al., 2012). Our finding that LIPUS stimulation enhances the Rac1-dependent migration of fibroblasts (Fig. 2D) is in accordance with *in vivo* data showing that daily LIPUS stimulation enhances fibroblast recruitment to skin wounds to promote healing in mice in a Rac1-dependent manner (Roper et al., 2015).

Mechanical stimulation by LIPUS is sensed by vinculin at FAs

How cells sense LIPUS stimulation to induce healing was one of the fundamental unknowns of the therapy. Previous reports showed that the 200 ms pulses produce nano-vibrations (Argadine et al., 2005; Harrison et al., 2016) as well as acoustic pressure (Fung et al., 2014), exposing cells to rapid mechanical stimuli.

In accordance with the proposed mechanism for how LIPUS stimulation works *in vivo* (Harrison et al., 2016), we show that integrin-mediated cell-ECM adhesions are essential for the cellular responses to LIPUS (Fig. 4), and that vinculin has a critical role in this process (Fig. 5). In the absence of vinculin, LIPUS fails to increase Rac1 activity, cell migration or endocytosis, all of which are cellular responses induced by LIPUS in WT cells (Fig. 5). Given

Journal of Cell Science (2017) 130, 2277-2291 doi:10.1242/jcs.192781

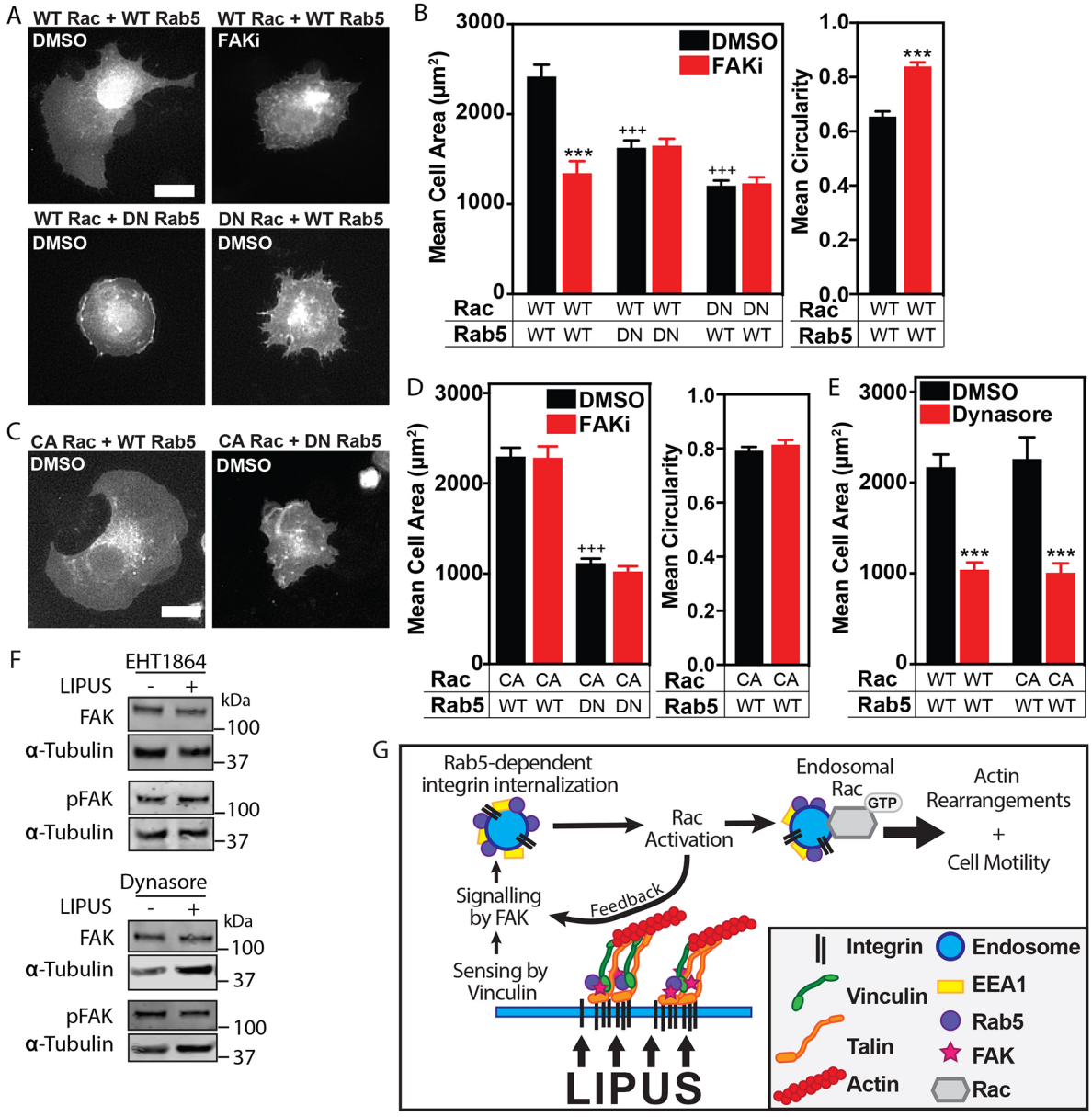

Fig. 8. A FAK-Rab5-Rac1 pathway mediates cell spreading and the response to LIPUS. (A) Representative images of B16 cells coexpressing the indicated constructs pretreated in suspension with either DMSO or FAKi for 1 h before being plated onto fibronectin and fixed after 45 min. Scale bar: 20 µm. (B) Measurements of mean cell area and mean cell circularity show that FAKi treatment reduces cell spreading, similar to expression of either $Rac1^{N17}$ (DN) or $Rab5^{N34}$ (DN). Data are mean±s.e.m. from three independent experiments; n=46–78. ***P<0.001 against the DMSO control; ^{+++}P<0.001 against WT Rac1 and WT Rab5-expressing DMSO control. (C) Representative images of B16 cells expressing $Rac1^{L61}$ (CA) with either WT Rab5 or $Rab5^{N34}$. Scale bar: 20 µm. (D) Quantification of the cell area shows that CA Rac1 expression rescues the defects in cell spreading associated with FAKi treatment. Coexpression of $Rab5^{N34}$ with $Rac1^{L61}$ reduces cell spreading to a similar extent to FAKi treatment. Data are mean±s.e.m. from three independent experiments; n=50–72. ^{+++}P<0.001 against CA Rac1 and WT Rab5-expressing DMSO control. (E) Mean cell area of B16 cells coexpressing the indicated Rac1 and Rab5 constructs, treated in suspension with either DMSO or dynasore. Note that dynasore treatment has a similar effect on cell area as coexpression of $Rab5^{N34}$. Data are mean±s.e.m. from three independent experiments; n=21–40. ***P<0.001 against DMSO control. (F) B16 cells treated with either EHT1864 (10 µM) or dynasore (80 µM) were stimulated for 10 min with LIPUS to assess pFAK-Y397 levels. Western blots show that inhibition of either Rac1 or dynamin blocks the LIPUS-induced increase in pFAK levels (blots are representative of at least three independent experiments; α-tubulin was used as a loading control). (G) Model of how cells sense and respond to LIPUS: LIPUS stimulation is 'sensed' by vinculin at integrin-mediated cell-ECM adhesions, requiring the link between vinculin and the actin cytoskeleton. FAK signalling leads to Rab5-dependent activation of Rac1. Once Rac1 is active, a feedback mechanism promotes further FAK phosphorylation, thereby propagating Rac1 activity. Active Rac1 localizes at Rab5-positive vesicles to facilitate trafficking, promoting rearrangements of the actin cytoskeleton and increased cell motility.

its known role in cellular mechanotransduction (Atherton et al., 2016; Schwarz and Gardel, 2012), and the finding that the actin binding potential of vinculin is essential for LIPUS sensing and the subsequent effects of enhanced endosome formation and cell motility (Fig. 5), our data suggest that vinculin acts as a mechanosensor of the small forces generated by LIPUS. The inability of cells lacking functional vinculin to respond to LIPUS stimulation resembles previous observations of cells subjected to cyclic stretching, where cells lacking vinculin, or expressing a tail-less vinculin construct, did not respond to the stimulus (Carisey

et al., 2013). LIPUS reduced vinculin mobility even in the presence of FAK inhibition (Fig. 6F), and we observed no increase in FAK phosphorylation upon LIPUS stimulation in vin$^{-/-}$ cells (Fig. 6G), suggesting that FAK acts downstream of vinculin. This is consistent with our recent findings that vinculin acts as a mechanosensor by changing its turnover rate in response to mechanical stimuli (in the form of different stiffnesses of the ECM substrate), independently of FAK activity (Stutchbury et al., 2017). Similarly, one cellular response to cyclic stretching is increased FAK phosphorylation (Sai et al., 1999; Wang et al., 2001), which likely occurs downstream of the initial sensing of the stimulus by vinculin. Precisely how this crosstalk between the mechanosensing protein vinculin and the signalling protein FAK occurs remains to be fully elucidated.

The finding that integrins colocalize with many of the endosomes (Fig. 7A,B) has put forward a model whereby the LIPUS-induced forces lead to internalization of the whole integrin-associated complex that proceeds to maintain a signalling function on the endosome, as has been suggested previously (Alanko et al., 2015; Palamidessi et al., 2008). This model is supported by our findings that many Rab5-positive endosomes contained activated Rac1 (Fig. S4F). MC3T3 cells cultured on collagen also showed an increase in motility after LIPUS stimulation (data not shown). That we did not observe any colocalization between GFP-α5 integrin and EEA1 in MEFs on collagen (Fig. S3G) suggests that integrin internalization after LIPUS stimulation only occurs when the receptor is bound to its ligand.

Rac1 activation occurs downstream of FAK signalling in a Rab5-dependent manner

Our finding that Rac1 activation occurs downstream of vinculin is in accordance with reports that vinculin controls localized Rac1 activity (Carisey et al., 2013). FAK is also involved in Rac1 activation in response to LIPUS, since pretreatment with a FAK inhibitor blocks Rac1 activation (Fig. 6A). Furthermore, we observed an increase in levels of pFAK-Y397 upon LIPUS stimulation (Fig. 6A). It is likely that FAK signalling to activate Rac1 occurs initially at FAs, rather than at integrin-containing endosomes, which have been reported to contain pFAK-Y397 (Alanko et al., 2015). However, pFAK-Y397 at this compartment could act to sustain Rac1 signalling once LIPUS stimulation has ended.

Cell spreading on fibronectin is both FAK dependent (FAKi treatment reduced cell area) (Fig. 8A,B) and Rac1 dependent (expression of Rac1^{N17} reduced cell area) (Fig. 8A,B). However, cells expressing Rac1^{L61} were unaffected by FAKi treatment, indicating that Rac1 activation occurs downstream of FAK signalling during cell spreading. Interestingly, coexpression of Rab5^{N34} with Rac1^{L61} reduced cell area, indicating that Rab5 is required for Rac1 activation in this FAK-mediated process, similar to what we find for Rac1 activation in response to LIPUS stimulation (Fig. 7C). Indeed, Rab5 has been shown to become activated upon integrin engagement with fibronectin during cell spreading (Torres et al., 2010).

In addition to expression of Rab5^{N34}, Rac1 activation in response to both LIPUS and cell spreading on fibronectin could be blocked by dynamin inhibition (Fig. 8E; Fig. S4A–C), suggesting that integrin internalization plays a role in activating Rac1 to facilitate cell spreading. Knockdown of the Rab5 GEF RIN2 reduces integrin internalization and Rac1 activation by ∼50% (Sandri et al., 2012). Conversely, knockout of the Rab5 GAP RN-Tre (also known as USP6NL) increases integrin internalization and cell migration (Palamidessi et al., 2013). These studies, together with our results presented here, clearly demonstrate a requirement for Rab5 in activating Rac1.

Interestingly, cells treated with the Rac1 inhibitor EHT1864 did not show any changes in pFAK-Y397 levels after 10 min of LIPUS stimulation (Fig. 8F). This suggests that although Rac1 activation occurs downstream of FAK signalling (Fig. 6C), this signalling is required to further increase FAK activation. Therefore, it may be the case that the initial activation of FAK in response to LIPUS occurs at focal complexes, which then activates Rac1 (indeed, we observed a small increase in pFAK-Y397 levels after 2 min of stimulation) (Fig. 6A). This then perpetuates further FAK signalling throughout the cell, thereby driving the response to LIPUS, and would explain why cells continue to migrate faster even when LIPUS stimulation has ended.

The link between adhesion proteins and Rab5

Interestingly, in nonstimulated cells, we observed greater Rac1-Rab5 colocalization in vin$^{-/-}$ MEFs than in cells expressing vinFL (Fig. 7F). Similarly, vin$^{-/-}$ MEFs had more EEA1-positive vesicles containing GFP-α5 integrin than cells rescued with vinculin (Fig. 7A,B). This is further evidence that integrin internalization and Rab5-mediated Rac1 activation or trafficking may contribute to cell migration, since vinculin-deficient cells also migrate faster than vinFL-expressing cells (Fig. 5B) (Saunders et al., 2006). Furthermore, our data suggest that vinculin has a role in controlling this process. Precisely how this occurs remains to be elucidated, but one possibility is that vinculin regulates Rab5 indirectly through Rab5-specific GEFs or GAPs. Both RIN2 (Sandri et al., 2012) and RN-Tre (Palamidessi et al., 2013) have been shown to localize to and regulate FAs. Importantly, RIN2 colocalizes with vinculin at adhesions and with vesicles containing both Rab5 and Rac1 (Sandri et al., 2012). Moreover, RIN2 regulates adhesion-dependent activation of Rac1 through the Rac1 GEF Tiam1 (Sandri et al., 2012), which is implicated in LIPUS-induced Rac1 activation (Roper et al., 2015) and the activation of Rac1 at Rab5-positive early endosomes (Palamidessi et al., 2008). This is particularly interesting, given that LIPUS stimulation promoted an increase in the number of Rab5-positive endosomes containing GTP-bound Rac1 (Fig. 7D,E; Fig. S4F).

The finding that Rab5 is proximal to FAs (Fig. S4J) is in agreement with a previously published report, which highlighted a role for Rab5 in modulating FA turnover (Mendoza et al., 2013). The same study demonstrated that cell migration promotes the formation of a complex of Rab5 with β1 integrin, FAK, paxillin and vinculin, and that FAs are enriched with GTP-bound Rab5 (Mendoza et al., 2013). Furthermore, associations between β1 integrin and Rab5 (Pellinen et al., 2006), and vinculin and Rab5 (Hagiwara et al., 2014), have been observed, pertinent to our findings that Rac1 activation requires both vinculin and Rab5, and that vinculin appears to regulate the behaviour and morphology of Rab5-positive vesicles (Fig. 7G,H; Movie 4). Further work is required to fully elucidate precisely how cell-ECM adhesion components regulate the Rab5-dependent activation of Rac1.

MATERIALS AND METHODS

Cell culture and transfections

Cells were cultured at 37°C with 5% CO_2, in Dulbecco's modified Eagle medium (DMEM) (B16s and MEFs) or α-MEM (MC3T3s), supplemented with 10% FCS, 1% L-glutamine and 1% nonessential amino acids. Transient transfections were performed using Lipofectamine and PLUS reagents (Life Technologies) as per the manufacturer's instructions.

Journal of Cell Science (2017) 130, 2277-2291 doi:10.1242/jcs.192781

Live imaging experiments were performed in Ham's F-12 medium (Sigma-Aldrich) lacking Phenol Red and riboflavin, supplemented with 1% glutamine, 1% penicillin/streptomycin and 25 mM HEPES.

Antibodies, reagents and plasmids

Bovine fibronectin (Sigma-Aldrich) was diluted in PBS to 10 µg/ml (unless indicated otherwise). Cell-Tak (BD Biosciences) was diluted in 0.1 M $NaHCO_3$ to a final concentration of 3.5 mg/cm^2, and coverslips were coated according to the manufacturer's instructions. When seeding onto Cell-Tak, cells were centrifuged twice in PBS with 10 mM EDTA to remove integrin-activating ions, and then seeded in serum-free medium.

EHT1864 (R&D Systems) was used at 10 µM with 4 h pretreatment. This concentration blocks the induction of PDGF-induced Rac1 activation (Shutes et al., 2007), suggesting that Rac1 activation is suppressed without affecting basal levels GTP-Rac1. This treatment was sufficient to block serum-induced actin reorganizations and motility (Fig. S1B). ML-141 (Sigma-Aldrich) was used at 10 µM with 1 h pretreatment. The FAK inhibitor AZ13256675 [Astra Zeneca; available from the pharmacology toolbox (http://openinnovation.astrazeneca.com/what-we-offer/pharmacology-toolbox/)] was diluted in DMSO and used at 3 µM with 1 h pretreatment.

Primary and secondary antibodies were diluted in 1% BSA (Sigma-Aldrich) before use. Antibodies used were as follows: rabbit anti-EEA1 (C45B10, 1:200, New England Biolabs), mouse anti-paxillin (clone 349, 1:400, BD Transduction Laboratories), Dylight 594 donkey anti-mouse IgG (1:500, Jackson ImmunoResearch) and Dylight 594 donkey anti-rabbit IgG (1:500, Jackson ImmunoResearch).

Stimulation with LIPUS

Cells were stimulated using an Exogen LIPUS device (Bioventus), emitting acoustic energy at a frequency of 1.5 MHz and pulse duration of 200 ms, pulsed at 1 kHz (Fig. S1A), giving an overall SATA of 30 mW/cm^2. Stimulation occurs for 20 min until the device automatically switches off. For fixed-cell experiments, cells seeded on glass coverslips in plastic wells were coupled to the device using a water-based gel and stimulated from below. For live-cell imaging, a single ultrasound transducer sterilized with 70% ethanol was placed into the medium, delivering LIPUS stimulation from above. Tracking of membrane protrusions was performed using the QuimP plugin for ImageJ (version 11b).

Circular dorsal ruffle assay

B16 GFP-actin cells were cultured overnight on fibronectin-coated glass coverslips. Cells were stimulated with LIPUS and fixed with 4% paraformaldehyde. To quantify CDR formation, images of randomly chosen XY positions were acquired using a Zeiss AxioObserver Z1 microscope with a 10×/0.3 NA objective. The total number of cells and the number of cells with CDRs in each image were counted manually, and used to calculate the percentage of cells with CDRs. For live-cell assays, cells were imaged using a Nikon TE2000 PFS microscope using a 40×/0.60 NA Plan Fluor objective and the Sedat Quad filter set (89000, Chroma). Images were acquired using a Cascade II EMCCD camera (Photometrics) every 60 s for 2 h, with LIPUS stimulation started at the end of the first hour. The number of CDRs formed by each cell in the first (control) and second (LIPUS) hour was counted.

Endosome quantification

Fixed cells were stained for EEA1. Images of the basal plane of cells were acquired using a Coolsnap HQ camera (Photometrics) on a DeltaVision (Applied Precision) microscope using a 60×/1.42 NA Plan Apo objective and the Sedat Quad filter set. Images were processed using ImageJ: first, background was subtracted using a rolling ball shape-based filter with an appropriate radius to isolate endosomes. Background-subtracted images were thresholded based on intensity to select endosomes (Fig. S2A). The number of early endosomes was quantified using the Particle Analysis function of ImageJ, set to detect structures between 0.1 and 0.3 µm^2.

Western blot quantification of FAK phosphorylation

Cells cultured overnight on fibronectin-coated plastic (10 µg/ml) in DMEM with 1% FCS were stimulated with LIPUS for the indicated amount of time, then washed with ice-cold PBS and lysed in RIPA buffer. 30 µg protein was loaded onto a 4–12% gradient gel. Protein was transferred to a nitrocellulose membrane and blotted for either FAK (rabbit polyclonal, AHO0502, 1:1000, Invitrogen), pFAK-Y397 (rabbit monoclonal, clone 141-9, 1:1000, Invitrogen) or α-tubulin (mouse monoclonal, clone DM1A, 1:1000, Sigma-Aldrich). Immunodetection was performed using an Odyssey imaging system using IRDye antibodies diluted 1:5000 (LI-COR Biosciences).

To determine levels of pFAK-Y397, samples were split and run on separate blots; one blot was stained for tubulin and total FAK, the other for tubulin and pFAK. Levels of both total FAK and pFAK were normalized to their respective tubulin stainings. Once normalized, a ratio was calculated to determine the amount of pFAK-Y397 relative to the amount of total FAK present in each lysate.

Cell spreading

B16 cells coexpressing the indicated GTPases were trypsinized and treated in suspension with either FAKi/DMSO (for 1 h) or dynasore/DMSO (for 10 min) as described above, then seeded onto glass coated with 10 µg/ml fibronectin. Cells were fixed 45 min after plating. Images were acquired using a Zeiss AxioObserver Z1 microscope with a 20×/0.4 NA objective; cell area and circularity measurements were performed using ImageJ.

Rac1 and Rab5 imaging and analysis

Cells coexpressing GFP-Rac1 and RFP-Rab5 were imaged using a spinning disk confocal microscope (CSU-X1, Yokogawa) supplied by Intelligent Imaging Innovations, equipped with a 60×/1.42 NA Plan Apo oil immersion objective (Zeiss). A 488-nm and a 561-nm laser were used to excite the GFP and RFP fluorophores, respectively. Images were captured using an Evolve EMCCD camera, and analysed using the JaCoP plugin for ImageJ (Bolte and Cordelieres, 2006). Colocalization analysis for GFP-α5 and EEA1 was performed the same way.

Live-cell movies of Rab5 were obtained using the above setup. Images were acquired every second for 60 s. To quantify vesicle speed, images were first corrected for bleaching using the Histogram Matching method, then background subtracted and auto-thresholded using the Otsu method to generate binary images, which were automatically tracked using the MTrack2 plugin for ImageJ.

FRET microscopy

Cells expressing the indicated Raichu FRET probe (Itoh et al., 2002; Yoshizaki et al., 2003) were cultured overnight on fibronectin-coated glass dishes (IBL). Images were acquired on a Nikon TE2000 PFS microscope with a heated stage and CO_2 supply using a 60×/1.40 NA Plan Apo objective with the Sedat Quad filter set and a Cascade II EMCCD camera (Photometrics). Donor images were acquired using a CFP excitation filter and a CFP emission filter; FRET images were acquired using a CFP excitation filter and a YFP emission filter.

Images were background subtracted using the 'Subtract from ROI' plugin of ImageJ, with an ROI drawn at the cell edge. Ratio images (FRET/Donor) were generated using the Image Calculator plugin of ImageJ, and the mean intensity over time of the resulting 32-bit float image was measured. Ratio measurements of each cell were normalized over time between 0 and 100 (% of total), and data were pooled. Bar graphs show the normalized values grouped from the indicated time points.

FLAP

FLAP experiments were performed as described previously (Atherton et al., 2015) in NIH3T3 cells cotransfected with the required PAGFP-tagged construct and mCherry-zyxin as a marker for FAs. Postactivation images were acquired every 10 s for 3 min. Images were acquired using the spinning disk confocal system described above. Photoactivation of PAGFP was achieved using a 405-nm laser for 5 ms; a 488-nm and a 561-nm laser were used to excite the GFP- and RFP-tagged proteins, respectively. Images were

analysed using a custom MATLAB algorithm as described previously (Atherton et al., 2015).

Cell migration

Cells were grown overnight on fibronectin-coated plastic in a medium supplemented with 1% FCS (limiting cell division). After LIPUS stimulation, cells were transferred to a preheated microscope chamber with a heated stage supplied with CO_2. For each condition, 5–10 XY positions were imaged every 10 min for 16 h using a Zeiss AxioObserver Z1 microscope equipped with a 10×/0.3 NA objective (Zeiss). Healthy, nondividing cells were tracked manually using ImageJ, and analysed using the Chemotaxis and Migration Tool plugin (Ibidi) for ImageJ to calculate velocity and directionality.

Graphs and statistical analysis

Statistical analyses were performed using Prism 6.0 (GraphPad). Differences between means were tested for significance using either a *t*-test (between two groups only), or a one-way ANOVA (between multiple groups) with a Tukey's posthoc test. Graphs were created using either Prism 6.0 or R 3.1.1 (R Foundation for Statistical Computing, Austria). Box plots show interquartile range, minimum and maximum values, median value and 95% confidence intervals of the median (notches); *n* numbers are indicated beneath box plots.

Acknowledgements

We thank the staff of the University of Manchester Bioimaging Facility, in particular Dr Peter March for his help and expertise with imaging, and Dr Egor Zindy for help with image analysis; Simon T. Barry (AstraZeneca) for providing the FAK inhibitor; and Ben Stutchbury, Dr Pat Caswell and Prof David Critchley for critical reading of the manuscript and helpful discussions. The QuimP plugins for ImageJ (Bosgraaf et al., 2009) were developed by Dr Till Bretschneider at the University of Warwick. Microscopes in the Bioimaging Facility of the Wellcome Trust Centre for Cell-Matrix Research, University of Manchester were purchased with grants from the BBSRC and Wellcome Trust, and a University of Manchester Strategic Fund.

Competing interests

A.H. is an employee of Bioventus that manufactures and sells a LIPUS device known as EXOGEN.

Author contributions

Conceptualization: P.A., C.B.; Methodology: P.A., C.B.; Formal analysis: P.A., F.L.; Investigation: P.A., F.L.; Data curation: P.A., F.L.; Writing - original draft: P.A.; Writing - review & editing: P.A., A.H., C.B.; Visualization: C.B.; Supervision: A.H., C.B.; Project administration: A.H., C.B.; Funding acquisition: A.H., C.B.

Funding

This study was supported by the Wellcome Trust (088785/Z/09/Z), Biotechnology and Biological Sciences Research Council (BBSRC; BB/J012254/1 to P.A.), Bioventus (P.A.) and Kids Kidney Research (F.L.). Deposited in PMC for release after 6 months.

Supplementary information

Supplementary information available online at
http://jcs.biologists.org/lookup/doi/10.1242/jcs.192781.supplemental

References

Alanko, J., Mai, A., Jacquemet, G., Schauer, K., Kaukonen, R., Saari, M., Goud, B. and Ivaska, J. (2015). Integrin endosomal signalling suppresses anoikis. *Nat. Cell Biol.* **17**, 1412-1421.

Argadine, H., Kinnick, R., Bolander, M. and Greenleaf, J. F. (2005). 1 kHz low power sound stimulates ATDC5 chondrocytes. *Proc. IEEE Ultrason Symp.* **2**, 996-998.

Atherton, P., Stutchbury, B., Wang, D.-Y., Jethwa, D., Tsang, R., Meiler-Rodriguez, E., Wang, P., Bate, N., Zent, R., Barsukov, I. L. et al. (2015). Vinculin controls talin engagement with the actomyosin machinery. *Nat. Commun.* **6**, 10038.

Atherton, P., Stutchbury, B., Jethwa, D. and Ballestrem, C. (2016). Mechanosensitive components of integrin adhesions: role of vinculin. *Exp. Cell Res.* **343**, 21-27.

Bae, Y. H., Mui, K. L., Hsu, B. Y., Liu, S.-L., Cretu, A., Razinia, Z., Xu, T., Pure, E. and Assoian, R. K. (2014). A FAK-Cas-Rac-lamellipodin signaling module transduces extracellular matrix stiffness into mechanosensitive cell cycling. *Sci. Signal.* **7**, ra57.

Ballestrem, C., Wehrle-Haller, B. and Imhof, B. A. (1998). Actin dynamics in living mammalian cells. *J. Cell Sci.* **111**, 1649-1658.

Ballestrem, C., Wehrle-Haller, B., Hinz, B. and Imhof, B. A. (2000). Actin-dependent lamellipodia formation and microtubule-dependent tail retraction control-directed cell migration. *Mol. Biol. Cell* **11**, 2999-3012.

Bolte, S. and Cordelieres, F. P. (2006). A guided tour into subcellular colocalization analysis in light microscopy. *J. Microsc.* **224**, 213-232.

Bosgraaf, L., van Haastert, P. J. M. and Bretschneider, T. (2009). Analysis of cell movement by simultaneous quantification of local membrane displacement and fluorescent intensities using Quimp2. *Cell Motil. Cytoskelet.* **66**, 156-165.

Brem, H., Golinko, M. S., Stojadinovic, O., Kodra, A., Diegelmann, R. F., Vukelic, S., Entero, H., Coppock, D. L. and Tomic-Canic, M. (2008). Primary cultured fibroblasts derived from patients with chronic wounds: a methodology to produce human cell lines and test putative growth factor therapy such as GMCSF. *J. Transl. Med.* **6**, 75.

Carisey, A., Tsang, R., Greiner, A. M., Nijenhuis, N., Heath, N., Nazgiewicz, A., Kemkemer, R., Derby, B., Spatz, J. and Ballestrem, C. (2013). Vinculin regulates the recruitment and release of core focal adhesion proteins in a force-dependent manner. *Curr. Biol.* **23**, 271-281.

Chan, Y.-S., Hsu, K.-Y., Kuo, C.-H., Lee, S.-D., Chen, S.-C., Chen, W.-J. and Ueng, S.-W. (2010). Using low-intensity pulsed ultrasound to improve muscle healing after laceration injury: an in vitro and in vivo study. *Ultrasound Med. Biol.* **36**, 743-751.

Cheng, K., Xia, P., Lin, Q., Shen, S., Gao, M., Ren, S. and Li, X. (2014). Effects of low-intensity pulsed ultrasound on integrin-FAK-PI3K/Akt mechanochemical transduction in rabbit osteoarthritis chondrocytes. *Ultrasound Med. Biol.* **40**, 1609-1618.

Dharmawardhane, S., Schurmann, A., Sells, M. A., Chernoff, J., Schmid, S. L. and Bokoch, G. M. (2000). Regulation of macropinocytosis by p21-activated kinase-1. *Mol. Biol. Cell* **11**, 3341-3352.

Dowrick, P., Kenworthy, P., McCann, B. and Warn, R. (1993). Circular ruffle formation and closure lead to macropinocytosis in hepatocyte growth factor/scatter factor-treated cells. *Eur. J. Cell Biol.* **61**, 44-53.

Ezratty, E. J., Bertaux, C., Marcantonio, E. E. and Gundersen, G. G. (2009). Clathrin mediates integrin endocytosis for focal adhesion disassembly in migrating cells. *J. Cell Biol.* **187**, 733-747.

Fu, S.-C., Hung, L.-K., Shum, W.-T., Lee, Y.-W., Chan, L.-S., Ho, G. and Chan, K.-M. (2010). In vivo low-intensity pulsed ultrasound (LIPUS) following tendon injury promotes repair during granulation but suppresses decorin and biglycan expression during remodeling. *J. Orthop. Sports Phys. Ther.* **40**, 422-429.

Fung, C.-H., Cheung, W.-H., Pounder, N. M., de Ana, F. J., Harrison, A. and Leung, K.-S. (2014). Investigation of rat bone fracture healing using pulsed 1.5 MHz, 30 mW/cm(2) burst ultrasound–axial distance dependency. *Ultrasonics* **54**, 850-859.

Gebauer, D., Mayr, E., Orthner, E. and Ryaby, J. P. (2005). Low-intensity pulsed ultrasound: effects on nonunions. *Ultrasound Med. Biol.* **31**, 1391-1402.

Geiger, B., Spatz, J. P. and Bershadsky, A. D. (2009). Environmental sensing through focal adhesions. *Nat. Rev. Mol. Cell Biol.* **10**, 21-33.

Goldmann, W. H. (2012). Mechanotransduction and focal adhesions. *Cell Biol. Int.* **36**, 649-652.

Hagiwara, M., Kokubu, E., Sugiura, S., Komatsu, T., Tada, H., Isoda, R., Tanigawa, N., Kato, Y., Ishida, N., Kobayashi, K. et al. (2014). Vinculin and Rab5 complex is required [correction of requited] for uptake of Staphylococcus aureus and interleukin-6 expression. *PLoS ONE* **9**, e87373.

Hanawa, K., Ito, K., Aizawa, K., Shindo, T., Nishimiya, K., Hasebe, Y., Tuburaya, R., Hasegawa, H., Yasuda, S., Kanai, H. et al. (2014). Low-intensity pulsed ultrasound induces angiogenesis and ameliorates left ventricular dysfunction in a porcine model of chronic myocardial ischemia. *PLoS ONE* **9**, e104863.

Harrison, A., Lin, S., Pounder, N. and Mikuni-Takagaki, Y. (2016). Mode & mechanism of low intensity pulsed ultrasound (LIPUS) in fracture repair. *Ultrasonics* **70**, 45-52.

Hauser, J., Ellisman, M., Steinau, H.-U., Stefan, E., Dudda, M. and Hauser, M. (2009). Ultrasound enhanced endocytotic activity of human fibroblasts. *Ultrasound Med. Biol.* **35**, 2084-2092.

Heckman, J. D., Ryaby, J. P., McCabe, J., Frey, J. J. and Kilcoyne, R. F. (1994). Acceleration of tibial fracture-healing by non-invasive, low-intensity pulsed ultrasound. *J. Bone Joint Surg. Am.* **76**, 26-34.

Higgins, A., Glover, M., Yang, Y., Bayliss, S., Meads, C. and Lord, J. (2014). EXOGEN ultrasound bone healing system for long bone fractures with non-union or delayed healing: a NICE medical technology guidance. *Appl. Health Econ. Health Policy* **12**, 477-484.

Holle, A. W., Tang, X., Vijayraghavan, D., Vincent, L. G., Fuhrmann, A., Choi, Y. S., del Álamo, J. C. and Engler, A. J. (2013). In situ mechanotransduction via vinculin regulates stem cell differentiation. *Stem Cells* **31**, 2467-2477.

Horton, E. R., Humphries, J. D., Stutchbury, B., Jacquemet, G., Ballestrem, C., Barry, S. T. and Humphries, M. J. (2016). Modulation of FAK and Src adhesion signaling occurs independently of adhesion complex composition. *J. Cell Biol.* **212**, 349-364.

Humphries, J. D., Wang, P., Streuli, C., Geiger, B., Humphries, M. J. and Ballestrem, C. (2007). Vinculin controls focal adhesion formation by direct interactions with talin and actin. *J. Cell Biol.* **179**, 1043-1057.

Hwang, D. S., Sim, S. B. and Cha, H. J. (2007). Cell adhesion biomaterial based on mussel adhesive protein fused with RGD peptide. *Biomaterials* **28**, 4039-4046.
Itoh, R. E., Kurokawa, K., Ohba, Y., Yoshizaki, H., Mochizuki, N. and Matsuda, M. (2002). Activation of rac and cdc42 video imaged by fluorescent resonance energy transfer-based single-molecule probes in the membrane of living cells. *Mol. Cell. Biol.* **22**, 6582-6591.
Jang, K. W., Ding, L., Seol, D., Lim, T.-H., Buckwalter, J. A. and Martin, J. A. (2014). Low-intensity pulsed ultrasound promotes chondrogenic progenitor cell migration via focal adhesion kinase pathway. *Ultrasound Med. Biol.* **40**, 1177-1186.
Jeremias Junior, S. L., Camanho, G. L., Bassit, A. C., Forgas, A., Ingham, S. J. and Abdalla, R. J. (2011). Low-intensity pulsed ultrasound accelerates healing in rat calcaneus tendon injuries. *J. Orthop. Sports Phys. Ther.* **41**, 526-531.
Katano, M., Naruse, K., Uchida, K., Mikuni-Takagaki, Y., Takaso, M., Itoman, M. and Urabe, K. (2011). Low intensity pulsed ultrasound accelerates delayed healing process by reducing the time required for the completion of endochondral ossification in the aged mouse femur fracture model. *Exp. Anim.* **60**, 385-395.
Kristiansen, T. K., Ryaby, J. P., McCabe, J., Frey, J. J. and Roe, L. R. (1997). Accelerated healing of distal radial fractures with the use of specific, low-intensity ultrasound. A multicenter, prospective, randomized, double-blind, placebo-controlled study. *J. Bone Joint Surg. Am.* **79**, 961-973.
Krueger, E. W., Orth, J. D., Cao, H. and McNiven, M. A. (2003). A dynamin-cortactin-Arp2/3 complex mediates actin reorganization in growth factor-stimulated cells. *Mol. Biol. Cell* **14**, 1085-1096.
Kusuyama, J., Bandow, K., Shamoto, M., Kakimoto, K., Ohnishi, T. and Matsuguchi, T. (2014). Low intensity pulsed ultrasound (LIPUS) influences the multilineage differentiation of mesenchymal stem and progenitor cell lines through ROCK-Cot/Tpl2-MEK-ERK signaling pathway. *J. Biol. Chem.* **289**, 10330-10344.
Lanzetti, L., Palamidessi, A., Areces, L., Scita, G. and Di Fiore, P. P. (2004). Rab5 is a signalling GTPase involved in actin remodelling by receptor tyrosine kinases. *Nature* **429**, 309-314.
Lu, H., Liu, F., Chen, H., Chen, C., Qu, J., Xu, D., Zhang, T., Zhou, J. and Hu, J. (2016). The effect of low-intensity pulsed ultrasound on bone-tendon junction healing: initiating after inflammation stage. *J. orthop. Res.* **34**, 1697-1706.
Mahoney, C. M., Morgan, M. R., Harrison, A., Humphries, M. J. and Bass, M. D. (2009). Therapeutic ultrasound bypasses canonical syndecan-4 signaling to activate rac1. *J. Biol. Chem.* **284**, 8898-8909.
Mendoza, P., Ortiz, R., Diaz, J., Quest, A. F. G., Leyton, L., Stupack, D. and Torres, V. A. (2013). Rab5 activation promotes focal adhesion disassembly, migration and invasiveness in tumor cells. *J. Cell Sci.* **126**, 3835-3847.
Merrifield, C. J., Moss, S. E., Ballestrem, C., Imhof, B. A., Giese, G., Wunderlich, I. and Almers, W. (1999). Endocytic vesicles move at the tips of actin tails in cultured mast cells. *Nat. Cell Biol.* **1**, 72-74.
Mizrahi, N., Zhou, E. H., Lenormand, G., Krishnan, R., Weihs, D., Butler, J. P., Weitz, D. A., Fredberg, J. J. and Kimmel, E. (2012). Low intensity ultrasound perturbs cytoskeleton dynamics. *Soft Mat.* **8**, 2438-2443.
Nolte, P. A., van der Krans, A., Patka, P., Janssen, I. M., Ryaby, J. P. and Albers, G. H. (2001). Low-intensity pulsed ultrasound in the treatment of nonunions. *J. Trauma* **51**, 693-702; discussion 702-693.
Onesto, C., Shutes, A., Picard, V., Schweighoffer, F. and Der, C. J. (2008). Characterization of EHT 1864, a novel small molecule inhibitor of Rac1 family small GTPases. *Methods Enzymol.* **439**, 111-129.
Owen, J. D., Ruest, P. J., Fry, D. W. and Hanks, S. K. (1999). Induced focal adhesion kinase (FAK) expression in FAK-null cells enhances cell spreading and migration requiring both auto- and activation loop phosphorylation sites and inhibits adhesion-dependent tyrosine phosphorylation of Pyk2. *Mol. Cell. Biol.* **19**, 4806-4818.
Padilla, F., Puts, R., Vico, L. and Raum, K. (2014). Stimulation of bone repair with ultrasound: a review of the possible mechanic effects. *Ultrasonics* **54**, 1125-1145.
Palamidessi, A., Frittoli, E., Garré, M., Faretta, M., Mione, M., Testa, I., Diaspro, A., Lanzetti, L., Scita, G. and Di Fiore, P. P. (2008). Endocytic trafficking of Rac1 is required for the spatial restriction of signaling in cell migration. *Cell* **134**, 135-147.
Palamidessi, A., Frittoli, E., Ducano, N., Offenhauser, N., Sigismund, S., Kajiho, H., Parazzoli, D., Oldani, A., Gobbi, M., Serini, G. et al. (2013). The GTPase-activating protein RN-tre controls focal adhesion turnover and cell migration. *Curr. Biol.* **23**, 2355-2364.
Paul, N. R., Jacquemet, G. and Caswell, P. T. (2015). Endocytic trafficking of integrins in cell migration. *Curr. Biol.* **25**, R1092-R1105.
Pellinen, T., Arjonen, A., Vuoriluoto, K., Kallio, K., Fransen, J. A. M. and Ivaska, J. (2006). Small GTPase Rab21 regulates cell adhesion and controls endosomal traffic of beta1-integrins. *J. Cell Biol.* **173**, 767-780.
Puklin-Faucher, E. and Sheetz, M. P. (2009). The mechanical integrin cycle. *J. Cell Sci.* **122**, 179-186.
Ridley, A. J. (2011). Life at the leading edge. *Cell* **145**, 1012-1022.
Roberts, M., Barry, S., Woods, A., van der Sluijs, P. and Norman, J. (2001). PDGF-regulated rab4-dependent recycling of alphavbeta3 integrin from early endosomes is necessary for cell adhesion and spreading. *Curr. Biol.* **11**, 1392-1402.
Roper, J. A., Williamson, R. C., Bally, B., Cowell, C. A., Brooks, R., Stephens, P., Harrison, A. J. and Bass, M. D. (2015). Ultrasonic stimulation of mouse skin reverses the healing delays in diabetes and aging by activation of Rac1. *J. Invest. Dermatol.* **135**, 2842-2851.
Rubashkin, M. G., Cassereau, L., Bainer, R., DuFort, C. C., Yui, Y., Ou, G., Paszek, M. J., Davidson, M. W., Chen, Y.-Y. and Weaver, V. M. (2014). Force engages vinculin and promotes tumor progression by enhancing PI3K activation of phosphatidylinositol (3,4,5)-triphosphate. *Cancer Res.* **74**, 4597-4611.
Rutten, S., Nolte, P. A., Guit, G. L., Bouman, D. E. and Albers, G. H. R. (2007). Use of low-intensity pulsed ultrasound for posttraumatic nonunions of the tibia: a review of patients treated in the Netherlands. *J. Trauma* **62**, 902-908.
Sai, X., Naruse, K. and Sokabe, M. (1999). Activation of pp60(src) is critical for stretch-induced orienting response in fibroblasts. *J. Cell Sci.* **112**, 1365-1373.
Sandri, C., Caccavari, F., Valdembri, D., Camillo, C., Veltel, S., Santambrogio, M., Lanzetti, L., Bussolino, F., Ivaska, J. and Serini, G. (2012). The R-Ras/RIN2/Rab5 complex controls endothelial cell adhesion and morphogenesis via active integrin endocytosis and Rac1 signaling. *Cell Res.* **22**, 1479-1501.
Sato, M., Nagata, K., Kuroda, S., Horiuchi, S., Nakamura, T., Karima, M., Inubushi, T. and Tanaka, E. (2014). Low-intensity pulsed ultrasound activates integrin-mediated mechanotransduction pathway in synovial cells. *Ann. Biomed. Eng.* **42**, 2156-2163.
Saunders, R. M., Holt, M. R., Jennings, L., Sutton, D. H., Barsukov, I. L., Bobkov, A., Liddington, R. C., Adamson, E. A., Dunn, G. A. and Critchley, D. R. (2006). Role of vinculin in regulating focal adhesion turnover. *Eur. J. Cell Biol.* **85**, 487-500.
Sawai, Y., Murata, H., Koto, K., Matsui, T., Horie, N., Ashihara, E., Maekawa, T., Fushiki, S. and Kubo, T. (2012). Effects of low-intensity pulsed ultrasound on osteosarcoma and cancer cells. *Oncol. Rep.* **28**, 481-486.
Schwarz, U. S. and Gardel, M. L. (2012). United we stand: integrating the actin cytoskeleton and cell-matrix adhesions in cellular mechanotransduction. *J. Cell Sci.* **125**, 3051-3060.
Sero, J. E., Thodeti, C. K., Mammoto, A., Bakal, C., Thomas, S. and Ingber, D. E. (2011). Paxillin mediates sensing of physical cues and regulates directional cell motility by controlling lamellipodia positioning. *PLoS ONE* **6**, e28303.
Shemesh, T., Geiger, B., Bershadsky, A. D. and Kozlov, M. M. (2005). Focal adhesions as mechanosensors: a physical mechanism. *Proc. Natl. Acad. Sci. USA* **102**, 12383-12388.
Shutes, A., Onesto, C., Picard, V., Leblond, B., Schweighoffer, F. and Der, C. J. (2007). Specificity and mechanism of action of EHT 1864, a novel small molecule inhibitor of Rac1 family small GTPases. *J. Biol. Chem.* **282**, 35666-35678.
Stutchbury, B., Atherton, P., Tsang, R., Wang, D. Y. and Ballestrem, C. (2017). Distinct focal adhesion protein modules control different aspects of mechanotransduction. *J. Cell Sci.* **130**, 1612-1624.
Sudo, H., Kodama, H. A., Amagai, Y., Yamamoto, S. and Kasai, S. (1983). In vitro differentiation and calcification in a new clonal osteogenic cell line derived from newborn mouse calvaria. *J. Cell Biol.* **96**, 191-198.
Suetsugu, S., Yamazaki, D., Kurisu, S. and Takenawa, T. (2003). Differential roles of WAVE1 and WAVE2 in dorsal and peripheral ruffle formation for fibroblast cell migration. *Dev. Cell* **5**, 595-609.
Surviladze, Z., Waller, A., Strouse, J. J., Bologa, C., Ursu, O., Salas, V., Parkinson, J. F., Phillips, G. K., Romero, E. and Wandinger-Ness, A., (2010). A Potent and Selective Inhibitor of Cdc42 GTPase. In Probe Reports from the NIH Molecular Libraries Program, Bethesda: National Center for Biotechnology Information.
Swaminathan, V., Fischer, R. S. and Waterman, C. M. (2016). The FAK-Arp2/3 interaction promotes leading edge advance and haptosensing by coupling nascent adhesions to lamellipodia actin. *Mol. Biol. Cell* **27**, 1085-1100.
Thievessen, I., Thompson, P. M., Berlemont, S., Plevock, K. M., Plotnikov, S. V., Zemljic-Harpf, A., Ross, R. S., Davidson, M. W., Danuser, G., Campbell, S. L. et al. (2013). Vinculin-actin interaction couples actin retrograde flow to focal adhesions, but is dispensable for focal adhesion growth. *J. Cell Biol.* **202**, 163-177.
Thompson, P. M., Tolbert, C. E., Shen, K., Kota, P., Palmer, S. M., Plevock, K. M., Orlova, A., Galkin, V. E., Burridge, K., Egelman, E. H. et al. (2014). Identification of an actin binding surface on vinculin that mediates mechanical cell and focal adhesion properties. *Structure* **22**, 697-706.
Torres, V. A., Mielgo, A., Barbero, S., Hsiao, R., Wilkins, J. A. and Stupack, D. G. (2010). Rab5 mediates caspase-8-promoted cell motility and metastasis. *Mol. Biol. Cell* **21**, 369-376.
Uddin, S. M., Richbourgh, B., Ding, Y., Hettinghouse, A., Komatsu, D. E., Qin, Y. X. and Liu, C. (2016). Chondro-protective effects of low intensity pulsed ultrasound. *Osteoarthritis Cartilage* **24**, 1989-1998.
Veronick, J., Assanah, F., Nair, L. S., Vyas, V., Huey, B. and Khan, Y. (2016). The effect of acoustic radiation force on osteoblasts in cell/hydrogel constructs for bone repair. *Exp. Biol. Med. (Maywood)* **241**, 1149-1156.
Wang, J. G., Miyazu, M., Matsushita, E., Sokabe, M. and Naruse, K. (2001). Uniaxial cyclic stretch induces focal adhesion kinase (FAK) tyrosine phosphorylation followed by mitogen-activated protein kinase (MAPK) activation. *Biochem. Biophys. Res. Commun.* **288**, 356-361.
Wei, F.-Y., Leung, K.-S., Li, G., Qin, J., Chow, S. K.-H., Huang, S., Sun, M.-H., Qin, L. and Cheung, W.-H. (2014). Low intensity pulsed ultrasound enhanced mesenchymal stem cell recruitment through stromal derived factor-1 signaling in fracture healing. *PLoS ONE* **9**, e106722.

Journal of Cell Science

Xia, P., Ren, S., Lin, Q., Cheng, K., Shen, S., Gao, M. and Li, X. (2015). Low-intensity pulsed ultrasound affects chondrocyte extracellular matrix production via an integrin-mediated p38 MAPK signaling pathway. *Ultrasound Med. Biol.* **41**, 1690-1700.

Yamashita, H., Ichikawa, T., Matsuyama, D., Kimura, Y., Ueda, K., Craig, S. W., Harada, I. and Kioka, N. (2014). The role of the interaction of the vinculin proline-rich linker region with vinexin alpha in sensing the stiffness of the extracellular matrix. *J. Cell Sci.* **127**, 1875-1886.

Yoshizaki, H., Ohba, Y., Kurokawa, K., Itoh, R. E., Nakamura, T., Mochizuki, N., Nagashima, K. and Matsuda, M. (2003). Activity of Rho-family GTPases during cell division as visualized with FRET-based probes. *J. Cell Biol.* **162**, 223-232.

Zhou, S., Schmelz, A., Seufferlein, T., Li, Y., Zhao, J. and Bachem, M. G. (2004). Molecular mechanisms of low intensity pulsed ultrasound in human skin fibroblasts. *J. Biol. Chem.* **279**, 54463-54469.

Zura, R., Della Rocca, G. J., Mehta, S., Harrison, A., Brodie, C., Jones, J. and Steen, R. G. (2015a). Treatment of chronic (>1 year) fracture nonunion: heal rate in a cohort of 767 patients treated with low-intensity pulsed ultrasound (LIPUS). *Injury* **46**, 2036-2041.

Zura, R., Mehta, S., Della Rocca, G. J., Jones, J. and Steen, R. G. (2015b). A cohort study of 4,190 patients treated with low-intensity pulsed ultrasound (LIPUS): findings in the elderly versus all patients. *BMC Musculoskelet. Disord.* **16**, 45.